Wildfire smoke drives population exposure to ozone pollution and unhealthy air quality days across the United States

Minghao Qiu[1,2#*], Yangmingkai Li[1#], Marissa Childs[3], Makoto Kelp[4], Xiaomeng Jin[5], Guanyu Huang[1,2,6], Mahdieh Danesh Yazdi[2,6], Yaguang Wei[7], Yuan Wang[8], Kai Chen[9,10]

1 School of Marine and Atmospheric Sciences, Stony Brook University, Stony Brook, NY, U.S.A.

2 Program in Public Health, Stony Brook University, Stony Brook, NY, U.S.A.

3 Department of Environmental & Occupational Health Sciences, University of Washington, Seattle, WA, U.S.A.

4 Department of Atmospheric Sciences, University of Utah, Salt Lake City, UT, U.S.A.

5 Department of Environmental Sciences, Rutgers, The State University of New Jersey, New Brunswick, NJ, U.S.A.

6 Department of Family, Population, and Preventive Medicine, Stony Brook University, Stony Brook, NY, U.S.A.

7 Department of Environmental Medicine, Icahn School of Medicine at Mount Sinai, New York, NY, U.S.A.

8 Department of Earth System Science, Stanford Doerr School of Sustainability, Stanford University, Stanford, CA, U.S.A.

9 Department of Environmental Health Sciences, Yale School of Public Health, New Haven, CT, U.S.A.

10 Yale Center on Climate Change and Health, Yale School of Public Health, New Haven, CT, U.S.A.

[#] These authors contributed equally.

[*] To whom correspondence should be addressed. E-mail: minghao.qiu@stonybrook.edu

Abstract

Wildfire smoke is an increasing threat to air quality and public health in the United States, affecting population exposure to multiple air pollutants, including ground-level ozone (O_3). Most prior studies have focused on smoke fine particulate matter ($PM_{2.5}$), but how smoke affects surface O_3 concentrations at a population scale is less well characterized. Much less is known about how smoke O_3 impacts the Air Quality Index (AQI) in comparison to smoke $PM_{2.5}$, or what this implies for regulatory attainment and population exposure. Here we quantify daily O_3 concentrations attributable to wildfire smoke (i.e., smoke O_3) across the contiguous U.S. from 2006 to 2023, using ensemble machine learning models that isolate the smoke contribution from meteorological variability. Smoke O_3 enhancement is widespread across all states, with the Midwest experiencing the largest increases. Wildfire smoke placed an additional 29 million people each year in areas exceeding the federal O_3 standard, and lengthened extreme O_3 episodes by 2.6 days on average. Smoke was responsible for 62.5% of person-days with unhealthy O_3 levels (defined as O_3 sub-index > 100) during 2021–2023. When smoke pushed the AQI into a worse category above 100, O_3 rather than $PM_{2.5}$ was the main pollutant 71.3% of the time. Smoke O_3 and smoke $PM_{2.5}$ are only weakly correlated and exhibit an inverted U-shaped relationship with substantial regional heterogeneity. Our results show that wildfire smoke is an increasingly important source of O_3 exposure and unhealthy air quality days, and that assessments based on $PM_{2.5}$ alone understate its air quality and health burden.

Significance Statement

Wildfire smoke threatens air quality and human health, but research on smoke exposure has focused largely on fine particulate matter ($PM_{2.5}$), with less attention to ground-level ozone (O_3). Using ensemble machine learning models trained on surface observations, we estimate daily smoke-driven O_3 across the contiguous United States, 2006–2023. Wildfire smoke has placed millions of additional people each year in areas exceeding the federal O_3 standard. In recent years, smoke has accounted for over 60% of days with unhealthy O_3 levels. On the poor air quality days caused by smoke, O_3 rather than $PM_{2.5}$ was the main pollutant more than 70% of the time. Health assessments and smoke advisories based on $PM_{2.5}$ alone therefore understate the burden of wildfire smoke.

Introduction

Increased wildfire activity across North America has led to a sharp rise in smoke pollution in the United States (*1–4*), which is becoming one of the most important health risk factors affecting U.S. populations (*5*, *6*). Exposure to wildfire smoke has been linked to emergency department visits for respiratory and cardiovascular disease (*7–9*), mental health conditions (*10*), and premature mortality (*11–14*). Quantifying these impacts at the population scale requires spatially complete exposure estimates at high resolution, going beyond the sparse coverage of surface monitoring network (*15*). Several gridded wildfire smoke exposure datasets have been developed for this purpose in the U.S. and globally (*2*, *16–19*). These datasets have supported research on health impacts and population exposure to wildfire smoke. Nearly all of this work, however, characterizes wildfire smoke through fine particulate matter ($PM_{2.5}$) alone. Because different pollutants form through different pathways and may not be closely correlated, a single-pollutant view may give an incomplete picture of the health risks and regulatory consequences of wildfire smoke. This is particularly true for ground-level ozone (O_3), a criteria pollutant regulated under the National Ambient Air Quality Standards (NAAQS), due to the large impacts from wildfires and the distinct formation pathway (*20–22*).

Wildfires can impact ground-level O_3 through emissions of precursor species (*23–25*), long-range transport (*26*, *27*), and radiative and chemical effects from smoke aerosols (*28*, *29*), with the net effect varying across space and time depending on the local chemical environment and meteorological conditions (*20*, *21*, *30–32*). Recent studies suggest that the wildfire impacts on O_3 are substantial and growing in the U.S. However, existing research has mostly quantified smoke contributions to ground-level O_3 over monitoring locations across the U.S. (*22*, *27*, *33–36*), or has developed gridded smoke O_3 data at local or regional scales (*37*, *38*). Xu et al. constructed a global gridded smoke O_3 dataset for 2000-2019, yet the smoke contribution is estimated from a global model which may not apply to the U.S. (*39*). In a recent paper, Deng et al. generated a 1-km gridded dataset of total O_3 concentrations across U.S. and estimated the wildfire smoke contribution in two ways: by excluding days and locations with anomalously high modeled carbon monoxide, or by scaling predicted O_3 by the fire fraction simulated in a chemical transport model (*15*). Using this dataset, they found that the long-term decline in total O_3 reversed after 2015, attributed to increasing fire emissions. However, excluding fire-affected days cannot separate smoke O_3 from other contributing factors such as co-varying meteorological conditions. Also, no study has compared smoke O_3 and smoke $PM_{2.5}$ contributions to air quality and health at the national scale.

Quantifying wildfire influences on population exposure to O_3 requires overcoming several methodological challenges that have been identified in the existing literature. Two general approaches have been used to estimate wildfire smoke contributions to air pollution and population exposure. The first relies on process-based chemical transport models (CTMs) driven by fire emissions inventories to simulate smoke pollutant concentrations (*40*, *41*). The second uses statistical or machine learning (ML) methods that relate surface observations to smoke indicators, remotely sensed atmospheric composition, fire, and meteorological predictors (*2*, *16–18*). Both approaches face important limitations for smoke O_3 estimations. CTMs are subject to high uncertainty in wildfire emissions inventories (*41*, *42*), and often rely on chemical mechanisms that may not adequately capture O_3 formation in smoke plumes (*43*). ML approaches can more closely reproduce observed surface pollution during smoke events, but may perform less well in areas with sparse monitoring coverage and may miss the impacts of diffuse smoke altogether (*44*). For ML approaches, accounting for meteorological conditions on smoke days is particularly important for O_3, as smoke days tend to have higher temperatures and greater UV radiation that separately promote O_3 formation (*22*).

In this study, we quantify wildfire smoke impacts on surface O_3 at daily and 10 km resolution across the contiguous U.S. from 2006 to 2023. To leverage the strengths of observation-based approaches while accounting for the meteorological confounding identified above, we train two sets of ensemble ML models (Figure 1): (1) a smoke model that predicts Maximum Daily 8-hour Average (MDA8) O_3 on smoke days, and (2) a non-smoke model that estimates counterfactual O_3 concentrations under the same meteorological conditions but in the absence of fire smoke. Smoke days are identified using satellite-derived smoke plumes generated from the National Oceanic and Atmospheric Administration (NOAA) Hazard Mapping System (HMS), with sensitivity analyses conducted using alternative smoke day definitions. Both models predict MDA8 O_3 concentrations from U.S. Environmental Protection Agency's (EPA) AirData repository using a rich set of predictors (Table S1). Smoke O_3 is defined as the difference between predicted O_3 and estimated counterfactual non-smoke O_3 on each smoke day. Using these daily smoke O_3 estimates, we quantify wildfire smoke contributions to population O_3 exposure and NAAQS nonattainment, and we compare smoke O_3 with smoke $PM_{2.5}$ to assess whether their impacts coincide in space and time. We then quantify how often smoke shifts the reported Air Quality Index (AQI) into a worse category, and how much of that shift is primarily related to smoke O_3. Compared with prior monitor-based estimates of smoke O_3 (*22*, *33–35*), our estimates provide spatially complete coverage over a longer time horizon. Compared with the recent product from Deng et al. (*15*), our estimates are directly constrained by observations across both smoke and non-smoke days and separate smoke impacts on O_3 from co-occurring meteorological variability.

Results

Model Performance and Validations

Our non-smoke ensemble model performs well across most of the contiguous U.S. in predicting MDA8 O_3 on non-smoke days using a spatial-block CV (Figure 1, Table S2, Figure S1). Performance remains similar under a more stringent 150 km spatial CV split (Figure S2), suggesting that our model generalizes to locations farther from training monitors. The strong out-of-sample performance of the non-smoke model, as well as the overlap in predictors between smoke and non-smoke days (Figure S3), provides confidence in its use for estimating counterfactual non-smoke O_3 on smoke days under observed meteorological conditions.

Our smoke ensemble model predicts MDA8 O_3 on smoke days with similarly high accuracy (Figure 1, Table S2, Figure S1). The smoke model achieves comparable performance to the non-smoke model across the eastern U.S. but performs worse in the western U.S. (Figures S2 and S4). The lower performance in the western U.S. may reflect O_3 formation in smoke plumes through complex photochemistry that depends on fire-emitted VOC speciation, fuel characteristics, plume age, and NO_x regimes (*20*, *43*). These factors are not directly captured by the fire-related predictors in our ML models, and most are available only from individual field campaigns rather than data products across the U.S. We find that including interpolated O_3 concentrations from nearby surface monitors (see Methods) as an additional predictor achieves higher predictive accuracy in the western U.S. (Figure S5), with interpolated O_3 as the most important feature (Figures S6 and S7). However, the heavy reliance on a single feature raises concerns about overfitting and spatial artifacts (Figure S8). Nevertheless, the general pattern and population-level exposure in predicted O_3 remain highly similar across interpolation and non-interpolation models (Figure S9). We therefore use the non-interpolation smoke model as our primary model for estimating smoke O_3. Importantly, we also find that the prediction bias of O_3 generally has the same sign in >85% of the monitor locations across both smoke and non-smoke models, resulting in lower bias when calculating smoke O_3 as the differences between the two sets of predictions (Figure S10).

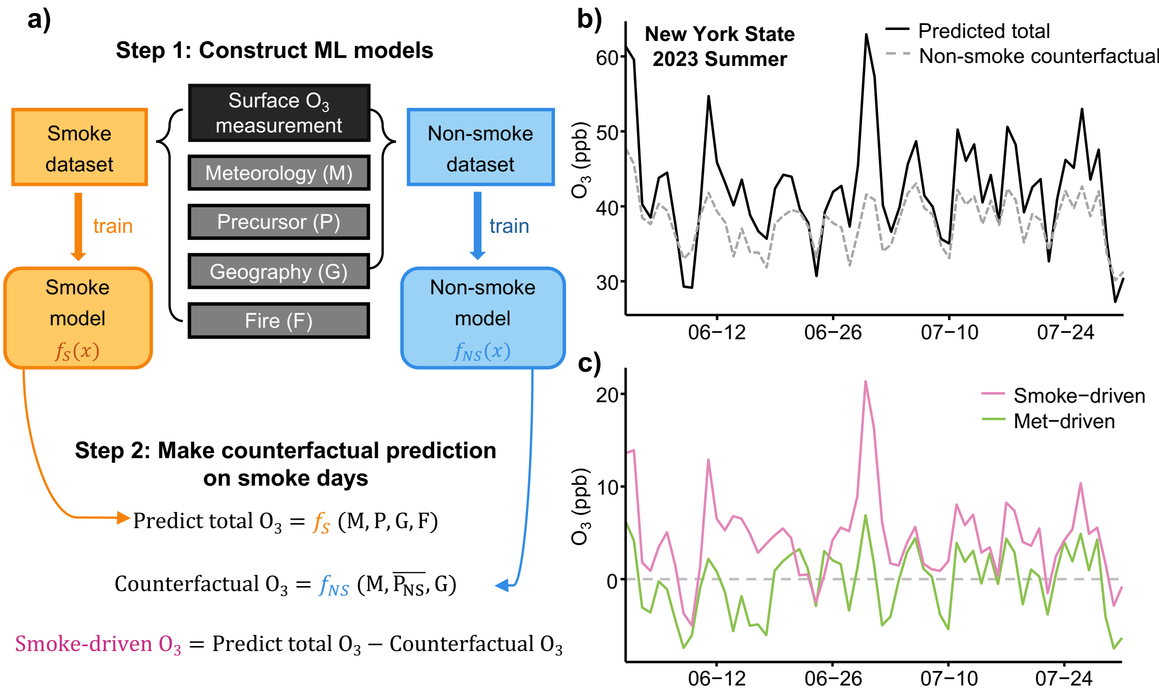

d)

Model	R^2	Within R^2	RMSE (ppb)	MAE (ppb)
Non-smoke (all-year)	0.73	0.57	7.28	5.47
Non-smoke (warm-season)	0.68	0.56	7.98	6.05
Smoke (no interpolation)	0.73	0.64	7.39	5.50
Smoke (with interpolation)	0.85	0.81	5.73	4.07

Figure 1: **Schematic figure of our machine learning-based approach for estimating smoke O_3 concentrations.** Panel a: In Step 1, we construct the smoke model to predict total O_3 concentration on smoke days, and the non-smoke model to predict total O_3 concentration on non-smoke days (thus used to predict counterfactual non-smoke O_3 on smoke days). In Step 2, we use these models to estimate the total O_3 concentration and counterfactual O_3 concentrations on smoke days. Panels b and c: an illustration of our method for New York State during summer 2023 (averaged over all grid cells in New York State). Panel b shows predicted total O_3 concentration ("predicted total", black line) and estimated counterfactual non-smoke O_3 using smoke-day meteorology (grey dashed line). Panel c: the plot shows smoke-driven O_3 changes (pink line) calculated as the difference between predicted total and counterfactual O_3, and met-driven O_3 changes (green line) calculated as the impacts of meteorological variability on O_3 concentrations. Panel d: out-of-sample performance metrics of smoke and non-smoke O_3 models, reported based on spatial cross-validation at 75 km resolution. Within R^2 is calculated from linear regressions that include station and month fixed effects. Warm season is defined as April to September.

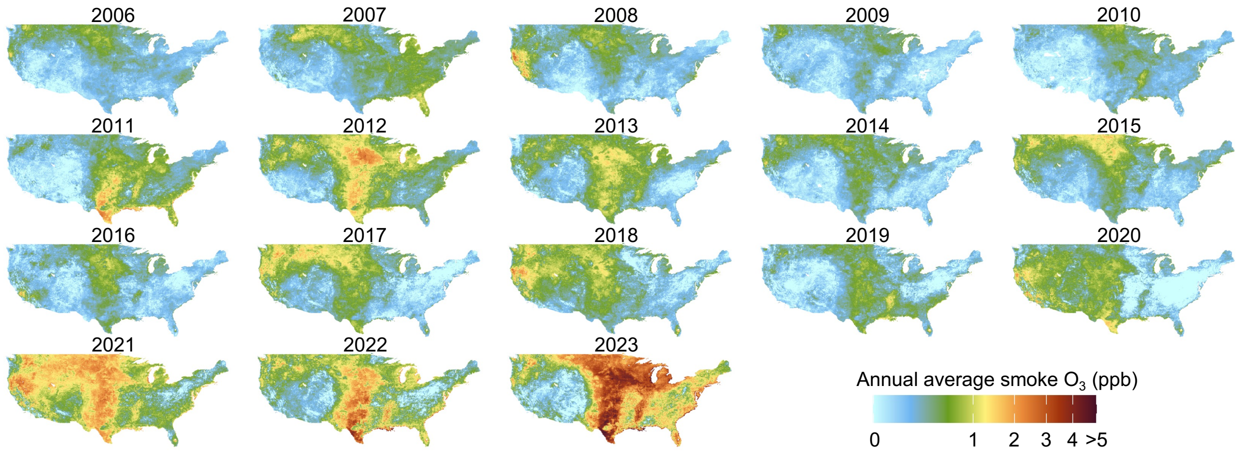

Figure 2: **Wildfire smoke contribution to annual average O_3 concentrations across the U.S. from 2006 to 2023.** Wildfire smoke contribution to annual average O_3 concentrations is calculated using "smoke-driven" O_3 estimates averaged over all days in a year (smoke O_3 is assumed to be zero on non-smoke days).

Wildfire smoke contribution to ground-level O_3

Wildfire smoke leads to widespread increases in surface O_3 across the contiguous U.S., with a growing contribution over time (Figure 2). These spatial patterns are broadly consistent with prior monitor-based estimates (*22*, *33*, *34*). During 2006-2022, smoke-driven O_3 enhancement was mostly observed in the western U.S., where wildfires are most active, and in the downwind Midwest. The Midwest consistently exhibits the highest smoke O_3 levels, as it is directly downwind of smoke from fires that occurred in the western U.S. and Canada. Wildfire smoke impacts on O_3 peaked in 2023, when the entire Midwest and Southern U.S., as well as parts of the Northeastern U.S., experienced elevated O_3 driven by widespread transport of Canadian wildfire smoke. Wildfire smoke increased the annual mean O_3 concentrations by up to 5 ppb in 2023 in the Midwest (see Figure S11 for modeled O_3 levels at selected stations in summer 2023). These results are consistent with prior analyses based on airborne and surface measurements over the Midwest during the 2023 Canadian smoke events (*27*, *36*).

We found that smoke has offset what would otherwise be a declining trend in population exposure to O_3 pollution across the U.S. We calculated the population-weighted O_3 "design value" (i.e., 3-year moving average of the 4th-highest annual MDA8 O_3 concentration) and the number of people living in nonattainment areas (O_3 design value exceeding 70 ppb), following the NAAQS criterion (Figure 3; Table S3). Absent smoke influence, the population-weighted O_3 design value would decline by

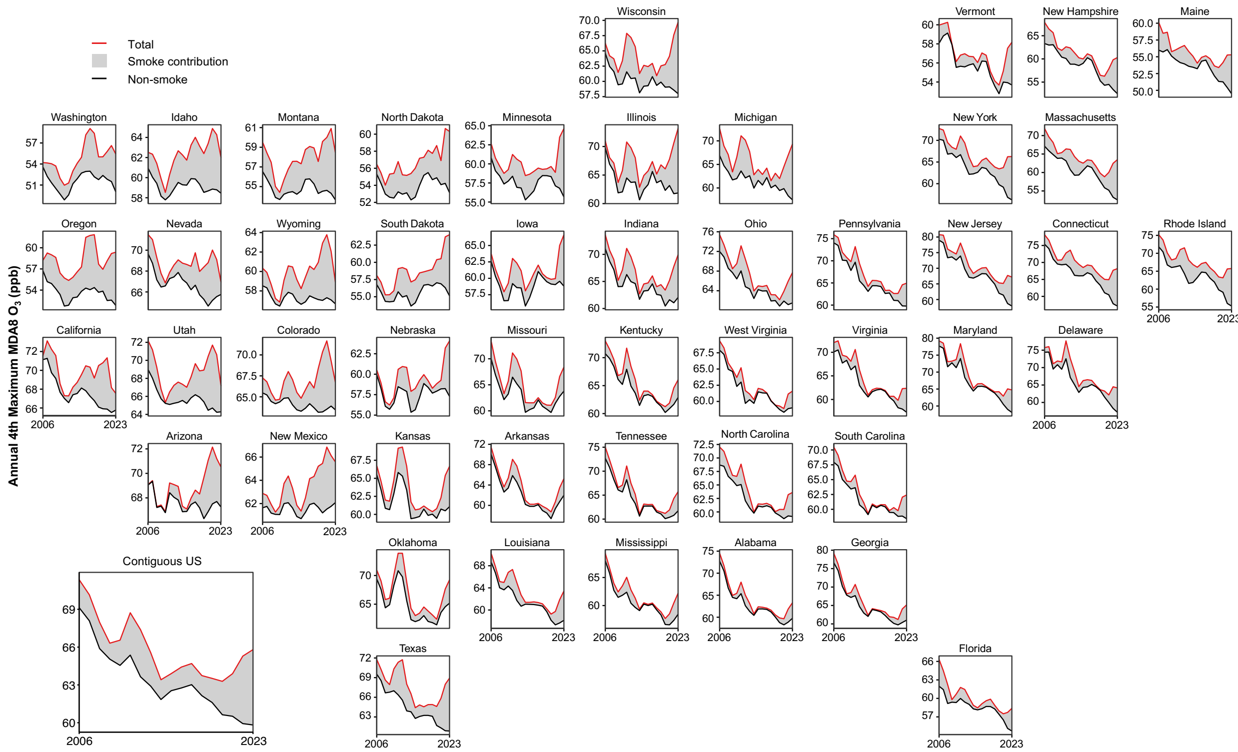

Figure 3: **The influence of wildfire smoke on population-weighted 3-year average 4th-highest MDA8 O_3 across U.S. states.** Lines show 3-year moving averages of population-weighted 4th-highest MDA8 O_3 for predicted total O_3 (red) and counterfactual non-smoke O_3 (black). Gray shading shows the smoke contribution, calculated by subtracting non-smoke O_3 from total O_3.

7.6 ppb at the national level (from 67.7 ppb in 2006-2008 to 60.1 ppb in 2021-2023), and the annual nonattainment population would fall from 95.7 million in 2006–2008 to 13.8 million in 2021–2023. We estimate that wildfire smoke has placed an additional 29 million people in nonattainment on average each year during 2006–2023, a 74% increase over the non-smoke baseline. Smoke-driven nonattainment regions are concentrated in the western U.S., Midwest, and northeastern U.S. (Figure S12). Smoke also contributes substantially to daily O_3 exceedance events, defined as days when MDA8 O_3 exceeds the 70 ppb NAAQS threshold (Figure S13).

Our estimates of smoke-driven O_3 isolated the contribution of fire smoke after accounting for the meteorological differences between smoke and non-smoke days. We found that not accounting for the meteorological variability between smoke and non-smoke days (e.g., higher ambient temperature and higher UV radiation on smoke days) would over-inflate our smoke O_3 estimates by 39% (Figure S14). Because wildfire smoke tends to occur under the same hot, sunny conditions that favor O_3

formation, smoke O_3 adds to days on which baseline O_3 is already high, exacerbating existing O_3 extremes. Wildfire smoke has lengthened O_3 extreme episodes (defined as at least two consecutive days on which the 3-day mean O_3 concentration exceeds 60 ppb) by an average of 2.6 days and raised the mean O_3 concentration during these episodes by 6.3 ppb (Figure S15). To better quantify smoke impacts on O_3 through different mechanisms, we further decomposed the smoke-driven O_3 into changes due to increases in O_3 precursors (using NO_2 and HCHO as proxies) and a residual component, by constructing an additional counterfactual prediction that allows NO_2 and HCHO concentrations to vary with smoke-day conditions (rather than using non-smoke average values). We found that changes in O_3 precursors account for 63% of the total smoke-driven O_3, with the remainder likely associated with direct transport of O_3 (*26*). Contributions from precursor changes almost dominate the smoke O_3 burden in regions closer to active fires (Figure S14).

Influences of smoke on AQI

We find that wildfire smoke contributes substantially to poor air quality days (defined as AQI>100) across the contiguous U.S. once its influence on both $PM_{2.5}$ and O_3 concentrations is accounted for (Figure 4). Of all person-days with AQI above 100 during 2006–2023 (including "Unhealthy for Sensitive Groups", "Unhealthy", "Very Unhealthy", and "Hazardous" categories), 41.7% are "smoke-driven". "Smoke-driven" AQI days are defined as days when the AQI category calculated from total $PM_{2.5}$ and O_3 concentrations is higher than the counterfactual category calculated from non-smoke $PM_{2.5}$ and non-smoke O_3 concentrations. In other words, the AQI category would have been lower without smoke contributions to $PM_{2.5}$ or O_3. The share of smoke-driven days is much higher for the worst air quality days. For example, all "Hazardous" days (AQI above 300) and 92.2% of "Very Unhealthy" days (AQI 201–300) are smoke-driven. As for O_3, 36.2% of bad O_3 days (sub-index above 100) are driven by smoke, and the percentage has increased to 62.5% during 2021-2023 and 75.7% during 2023 (Figure S16).

Importantly, the influence of smoke on O_3 is a major contributor to smoke impacts on the overall AQI, especially in the middle of the AQI range. Among smoke-driven days with AQI above 100, 71.3% have their category set by smoke O_3 alone, meaning those days would have been classified in a lower tier had we ignored smoke impacts on O_3. "Hazardous" days, by contrast, are driven entirely by smoke $PM_{2.5}$, because the 8-hour O_3 sub-index cannot exceed 300 and so cannot by itself produce a "Hazardous" classification (*45*). Given the importance of the AQI for public perception and for guiding public health recommendations, we further quantify the risk of misclassifying the AQI if

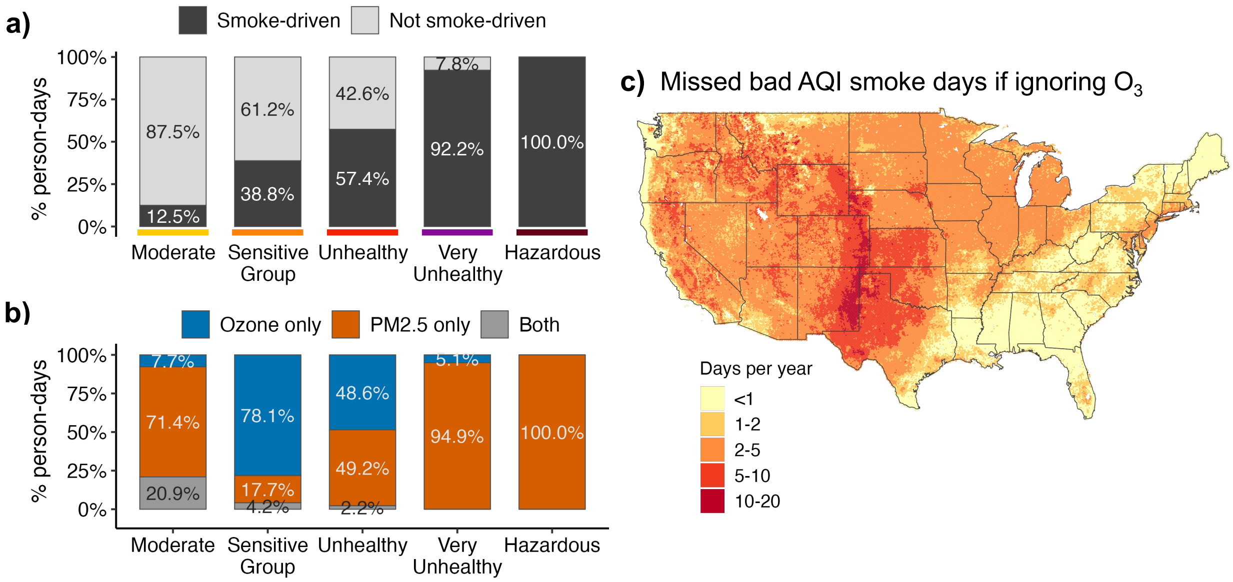

Figure 4: **Effects of smoke $PM_{2.5}$ and O_3 on AQI**. Panel a: percentage of smoke-driven and not smoke-driven person-days in each of five AQI categories (x-axis), 2006–2023. Panel b: among smoke-driven person-days, the percentage in which the AQI category is determined by $PM_{2.5}$ alone ($PM_{2.5}$ only), by O_3 alone (Ozone only), or by both pollutants (Both) meaning the AQI classification is the same. Panel c: the number of bad smoke days per year (defined with AQI > 50) that would be missed if the contribution of smoke to O_3 were ignored, i.e., if only smoke $PM_{2.5}$ were considered.

only smoke $PM_{2.5}$ is considered and O_3 is ignored. In reality, AQI is always calculated using actual concentrations of all pollutants; thus the exercise here is designed to quantify the contribution of O_3 to smoke impacts on air quality, and is more applicable in scenarios where smoke O_3 information is not available (e.g., air quality forecasts). We find that such misclassification is most severe in the AQI ranges 101–150 and 151–200 (Figure 4). For example, 72.6% of person-days in the "Unhealthy for Sensitive Groups" category would be labeled "Moderate" and 5.5% would be labeled "Good" if only smoke $PM_{2.5}$ impacts were considered (Figure S17). Similarly, 42.5% of person-days in the "Unhealthy" category would be labeled "Moderate". If we assume that people only pay attention to $PM_{2.5}$, this suggests that many would not have taken the protective actions the true air quality warranted. Averaged over 2006–2023, many locations experience at least one such missed day per year if smoke O_3 is ignored, most of them in the Midwest, Southwest, and Northeast (Figure 4).

Relationship between smoke $PM_{2.5}$ and smoke O_3

We found a non-linear and spatially heterogeneous relationship between smoke $PM_{2.5}$ and smoke O_3 across the contiguous U.S. (Figure 5). At the national level, daily smoke O_3 increases with smoke $PM_{2.5}$ up to a tipping point of approximately 60–70 μg/m^3 of daily smoke $PM_{2.5}$, beyond which smoke O_3 declines with further increases in smoke $PM_{2.5}$. This inverted U-shaped pattern is consistent with the documented effects that high smoke aerosol loading can suppress photochemical O_3 production by reducing light transmission and increasing HO_2 uptake, though existing evidence is mostly in the western U.S. (*28*, *29*). However, not all regions exhibit this pattern. In the Upper Midwest, Ohio Valley, South, and Southeast, smoke O_3 increases consistently with smoke $PM_{2.5}$ across the range of historically observed concentrations, with no evidence of a tipping point within observed levels. Even among regions that do exhibit an inverted U-shape, the tipping point varies substantially. We note that the spread of smoke O_3 within each smoke $PM_{2.5}$ bin is large (Figure 5), indicating that smoke $PM_{2.5}$ alone explains only a small fraction of the variation in smoke O_3. Overall, smoke $PM_{2.5}$ and smoke O_3 are only weakly correlated (with varying correlations across different smoke $PM_{2.5}$ ranges; Figure S18), suggesting that high smoke $PM_{2.5}$ exposure does not reliably predict high smoke O_3 exposure.

Smoke O_3 affected nearly all populations across the contiguous U.S., but meaningful differences in exposure exist across racial, ethnic, and income groups (Figure 6). For smoke O_3 exposures, Black populations face the highest exposure nationally (0.39–0.44 ppb across income deciles), followed by White (0.39–0.41 ppb), Hispanic (0.36–0.41 ppb), and Asian populations (0.33–0.37 ppb). A weak income gradient is present for most groups, with lower-income populations facing slightly higher smoke O_3 exposure. White populations are an exception and their smoke O_3 exposure is largely flat across income deciles. These distributional results differ from smoke $PM_{2.5}$ patterns, where White populations face the highest exposure (0.53–0.57 μg/m^3) and Hispanic populations face the lowest (0.47–0.51 μg/m^3). These contrasting patterns are driven by the different spatial distributions of the two pollutants combined with the geographic distribution of racial and income groups (Figures S19 and S20). In the western U.S. (defined as locations west of the meridian 100° west), where smoke $PM_{2.5}$ is highest, White populations face the greatest exposure to both pollutants. In the eastern U.S., where smoke O_3 is larger, Hispanic populations face the highest smoke O_3 exposure (0.47–0.52 ppb), while racial differences in smoke $PM_{2.5}$ are smaller. Prior studies have documented that wildfire smoke $PM_{2.5}$ exposure disparities do not follow conventional environmental justice patterns observed for non-smoke pollution (*16*, *46*, *47*). Our results suggest that considering smoke O_3 alongside smoke $PM_{2.5}$ adds further complexity to smoke exposure disparities.

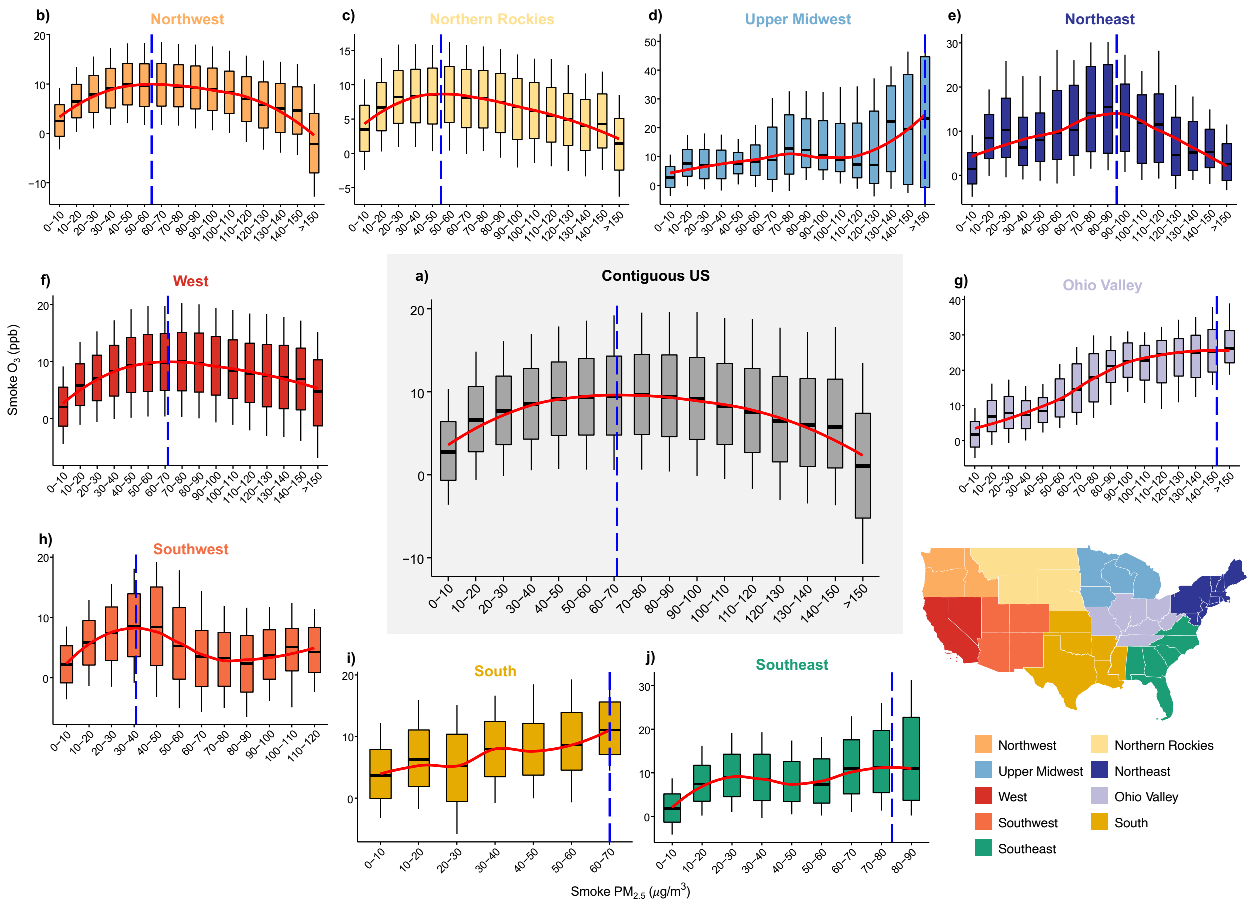

Figure 5: **National and regional patterns of non-linear relationships between smoke $PM_{2.5}$ and smoke O_3.** The boxplots illustrate the distributions of daily smoke O_3 within each daily smoke $PM_{2.5}$ bin: thick black lines represent the medians, box edges denote the 25th and 75th percentiles, and whiskers extend to the 10th and 90th percentiles. The solid red lines represent a LOESS regression fitted to the medians of each box. The vertical dashed blue lines indicate the smoke $PM_{2.5}$ threshold at which smoke O_3 concentrations reach their maximum value.

Discussion

In this study, we quantify the important and increasing contribution of wildfire smoke to U.S. O_3 trends and associated influence on population exposure and AQI. We found that wildfire smoke O_3 offset the otherwise declining trend in O_3 exposure and nonattainment populations over the study period. Smoke O_3 enhancement was widespread across the contiguous U.S. in recent years, with the Midwest experiencing the largest increases; this additional O_3 burden affected populations across all income and racial groups. The gridded smoke O_3 dataset we developed fills an important gap in existing smoke exposure products, which have focused almost exclusively on smoke $PM_{2.5}$ (*2*,

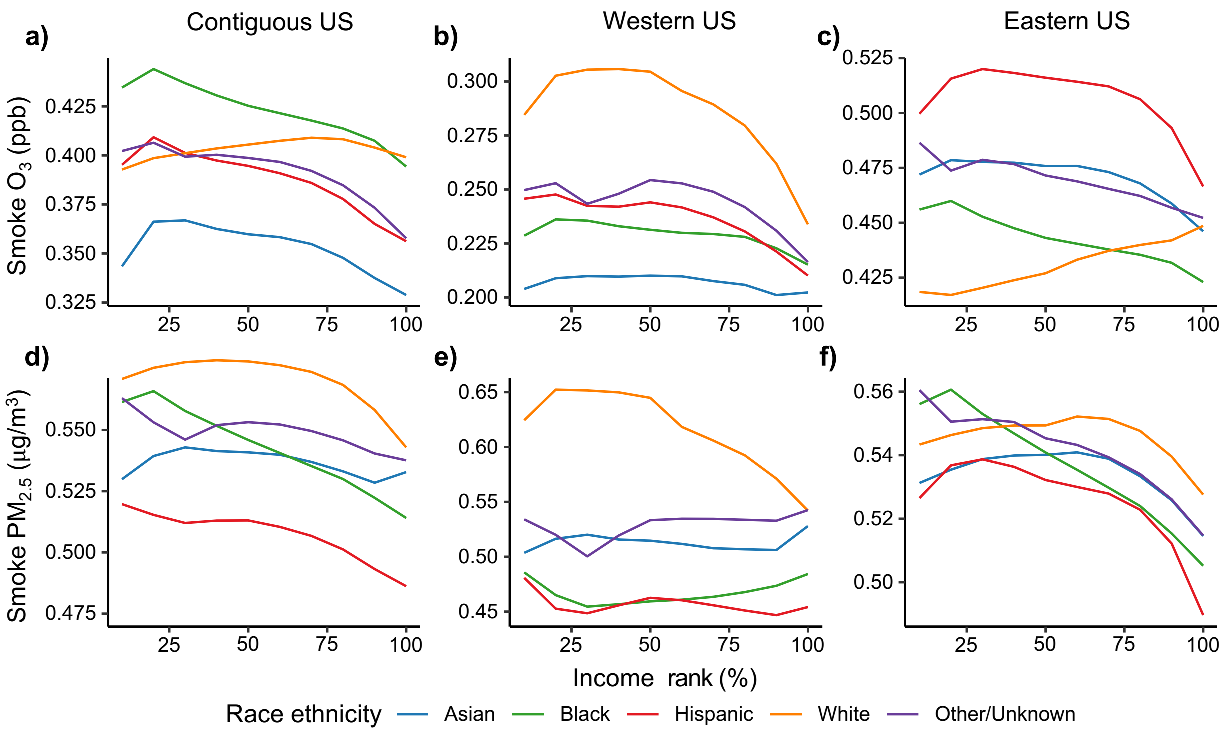

Figure 6: **Disparities in smoke O_3 and smoke $PM_{2.5}$ exposure by race/ethnicity and income groups.** Panels **a–c** show the average exposure to smoke O_3 across income rank (0–100%) and race or ethnicity (Asian, Black, Hispanic, White, and Other/Unknown) for the contiguous U.S., western U.S., and eastern U.S. The western U.S. is defined as locations west of the meridian 100° west. Panels **d–f** illustrate the corresponding exposure to smoke $PM_{2.5}$ for the same geographic regions.

16–18). Our findings extend prior monitor-based estimates of smoke O_3 (*22*, *33–35*) by providing spatially complete coverage that captures smoke O_3 in areas without surface monitors. The dataset also complements existing gridded total O_3 products by separating the wildfire smoke contribution from background O_3 (*15*, *48*).

Wildfire smoke influences on surface O_3 levels are highly complex, and our new gridded dataset provides a basis for investigating the underlying drivers of smoke O_3 at large regional scales. For example, future research could examine how smoke's effect on surface O_3 varies with fire and fuel characteristics, plume age, and the underlying O_3 chemistry regime. In constructing the smoke O_3 dataset, we carefully control for meteorological variability between smoke and non-smoke days, given that prior studies have shown that differences in ambient temperature and UV radiation between smoke and non-smoke days can substantially affect surface O_3 estimates (*22*). We also note that our approach treats all meteorological differences between smoke and non-smoke days as confounding factors to be accounted for. However, intense smoke events can themselves modify local meteorological conditions such as surface temperature and boundary layer height (*49*, *50*), suggesting that some portion of what we attribute to meteorological variability may itself be smoke-driven. Disentangling the direct effects of smoke on O_3 from these indirect meteorological pathways remains a challenge.

Our results indicate that smoke O_3 represents a distinct exposure that may not be well captured by smoke $PM_{2.5}$ alone. We find that smoke O_3 is responsible for a large share of smoke-driven poor air quality days, particularly in the AQI range 101-200. Consistent with prior monitor-based studies (*22*, *28*), we find that smoke O_3 and smoke $PM_{2.5}$ exhibit a complex inverted U-shaped relationship at the national level. A novel finding is that this relationship is regionally heterogeneous. The smoke $PM_{2.5}$–O_3 relationship also varies with distance from fires (Figure S21), consistent with the fact that O_3 is a secondary pollutant whose formation depends on plume age and the local chemical environment (*20*, *31*). These results suggest that health risk assessments for wildfire smoke would benefit from incorporating O_3, particularly in regions where the relationship between the two pollutants is weakest. Epidemiological studies using multi-pollutant smoke exposure data are needed to identify the additional health risks attributable to wildfire smoke O_3 and to characterize potential interactions between smoke O_3 and smoke $PM_{2.5}$ (*51*, *52*).

The smoke O_3 estimates could be improved in several ways. First, following prior literature, our analysis relies on HMS smoke plumes for smoke day classification, which carries known uncertainties in representing surface-level smoke influence (*34*, *44*, *53*). In sensitivity tests, we exclude HMS-identified smoke days when there is no significant increase in estimated surface smoke $PM_{2.5}$ (*16*). If we remove all days with estimated smoke $PM_{2.5}$ less than 1 μg/m^3 (which accounts for 22% of all smoke days), our estimated population exposure to smoke O_3 and the smoke-driven nonattainment populations only decrease by 2% (Figure S22). Thus, our estimated smoke contribution to O_3 exposure is largely robust to uncertainty in the smoke day identification. Second, simulations from CTMs could complement our ML approach by providing alternative smoke day identifications when satellite imagery is missing or uncertain during extreme smoke events. CTM simulations can also represent the non-linear O_3 chemistry regimes that our empirical models cannot directly capture (*43*). Third, incorporating additional fire-related variables such as fuel type and fire dynamics may help improve prediction performance, particularly in the western U.S. where our models perform less well. Synoptic weather patterns and fine-scale meteorological features such as sea breeze circulations could also be incorporated as predictors (*54*, *55*).

The wildfire smoke O_3 dataset we created, together with the accompanying non-smoke O_3 predictions, can support a range of research and policy analyses. The dataset enables multi-pollutant epidemiological studies of both long-term and short-term health effects of wildfire smoke (*7*, *37*). Our estimates of smoke-driven O_3 exceedance can inform policy discussions about exceptional events under the Clean Air Act (*56*, *57*). The dataset can also support research on smoke O_3 effects on agriculture and ecosystems (*58*) considering the known impacts of O_3 on plants. As wildfire smoke is projected to continue increasing under future climate change (*14*, *59*, *60*), these impacts from smoke O_3 are likely to grow substantially without adaptation policies to mitigate them. Using high-resolution datasets to map impacts of smoke O_3 is an important and necessary step to further design and evaluate the interventions and adaptation strategies.

Materials and Methods

Datasets

For surface O_3 observations, we obtained daily maximum 8-hour average ozone (MDA8 O_3) across monitoring stations from the U.S. Environmental Protection Agency's (EPA) AirData repository (*61*). We used a variety of public datasets for smoke and fire information. We used smoke plume polygons generated from the National Oceanic and Atmospheric Administration (NOAA) Hazard Mapping System (HMS) from 2006 to 2023. Smoke polygons are generated daily using near-real-time visible satellite imagery to delineate the spatial distribution of wildfire smoke over the contiguous U.S. (*62*, *63*). We used gridded daily wildfire smoke $PM_{2.5}$ estimates for the contiguous U.S. at 10 km resolution from 2006 to 2023 from Childs et al. (*16*, *56*). Childs et al. constructed XGBoost models using satellite-derived smoke plume, remotely sensed atmospheric variables, interpolations of $PM_{2.5}$ measurements from surface monitors, meteorological variables, and fire variables to predict anomalous increases in surface $PM_{2.5}$ during wildfire events. For fire information, we used the Moderate Resolution Imaging Spectroradiometer (MODIS) Active Fire products (Collection 6) from 2006 to 2023 across the U.S. to identify fire point locations and fire radiative power (FRP) (*64*), as provided by NASA's Fire Information for Resource Management System (FIRMS) (*65*). Fire pixels within a 20 km radius are aggregated into a single fire event, with the event center computed as the weighted mean of the fire pixel locations based on FRP (*23*, *24*).

Surface nitrogen dioxide (NO_2) and formaldehyde (HCHO) data from a global reanalysis product are used as indicators of O_3 precursors. The Copernicus Atmosphere Monitoring Service (CAMS)

Global Reanalysis, known as EAC4, is a comprehensive dataset of atmospheric composition produced by the European Centre for Medium-Range Weather Forecasts (ECMWF). It integrates a wide array of satellite observations with atmospheric modeling through data assimilation, providing consistent, three-dimensional global fields of various atmospheric constituents (*66*). The EAC4 product, available since 2003, provides global atmospheric data at a spatial resolution of 0.75 degree and a temporal resolution of 3 hours.

Meteorological data are sourced from both ERA5 and ERA5-Land products (*67*, *68*). We used daily ERA5-Land meteorological variables from 2006-2023 with a spatial resolution of 9 km, including 2m air temperature and dewpoint temperature (daily minimum, maximum, and mean), surface pressure, 10m v-component and u-component of wind, precipitation, surface (0-7cm) soil moisture, and leaf area index (high and low vegetation). Mean sea level pressure, surface downward UV radiation, cloud cover, column ozone, and boundary layer height are derived from ERA5 with a spatial resolution of 25 km. We used elevation data from EarthEnv, a 1 km digital elevation model synthesized from global terrain data (*69*). Land cover classification is derived from the MODIS MCD12C1 product, which categorizes the global surface into 17 distinct types defined by the International Geosphere-Biosphere Programme at 0.05 degree resolution (*70*). Population data are derived from the Gridded Environmental Impacts Frame (Gridded EIF) developed by the U.S. Census Bureau and released in February 2025. The dataset includes detailed demographic counts by age, sex, race, ethnicity, and household income decile on a fixed 0.01-degree grid in North America (*71*).

Smoke and non-smoke ML models

To estimate smoke contribution to surface O_3 concentrations, we developed two sets of ML models – referred to as “smoke models” and “non-smoke models” to predict daily MDA8 O_3 concentration (Figure 1). Observational samples are classified into smoke and non-smoke datasets, based on the presence of HMS smoke plumes following prior methods (*16*, *33*, *34*). The smoke models use input variables from five categories: meteorological variables, O_3 precursor variables, geographical variables, fire-related variables, and interpolated O_3 concentrations from monitored data. The non-smoke models use all input features above except for fire-related variables and interpolated O_3 concentrations. A comprehensive list of features used in model training is provided in Table S1.

We constructed separate smoke and non-smoke ML models using three algorithms: eXtreme Gradient Boosting (XGBoost) (*72*), Categorical Boosting (CatBoost) (*73*), and Neural Network

(NN). To further enhance the predictive accuracy and robustness of our O_3 estimations, we implemented a stacking ensemble approach (*48*). This method integrates outputs of the three individual ML models by using their predictions as input features for a meta-learner. Specifically, we employed a Random Forest algorithm as the meta-learner to capture complex, non-linear relationships among the base model predictions. By combining multiple base learners, the ensemble model mitigates the biases inherent in individual models and leverages their complementary strengths, leading to improved generalization performance.

ML models' hyperparameters are tuned via 5-fold cross-validation (CV), using regression with Root Mean Squared Error (RMSE) as the objective function. Note that we construct two versions of the smoke models: one incorporating all variables, including interpolated O_3 concentrations from EPA stations, and another excluding the interpolated O_3 concentrations. Here, the interpolated O_3 is calculated using inverse-distance weighting (IDW) spatial interpolation, based on ground-level O_3 observations from EPA monitoring stations. For each smoke day and each grid cell, we interpolate O_3 using all available monitor observations (*56*).

Model Evaluations

We evaluated the model performance using 5-fold spatial CV. To address the concerns of information leakage between the training and test sets, we split data by station locations, rather than using a conventional random split by observation (where a given station could contribute data to both sets). The spatial folds (disjoint sets of training and testing) are defined from the coarsest input (CAMS, ~75 km) to avoid further information leakages. Model performance is also assessed with a spatial split at 150 km to quantify its performance in regions with sparse monitor coverage. As discussed in prior literature, spatial CV provides a more realistic assessment of the model's ability to predict MDA8 O_3 at new locations with no surface observations (*16*, *74*). We reported four evaluation metrics: R^2, within R^2, RMSE, and Mean Absolute Error (MAE) on the held-out test set. Within R^2 is calculated by regressing observed MDA8 O_3 on predicted MDA8 O_3, including fixed effects for each station and month, thereby isolating within-location temporal variation. We employed SHapley Additive exPlanations (SHAP) (*75*) to enhance the interpretability of our ML models and understand the contribution of each feature to the predicted MDA8 O_3 concentrations (Figures S6 and S7).

Predicting smoke O_3

To generate grid-level smoke O_3 estimates, we used our smoke and non-smoke models to predict O_3 on each smoke day and non-smoke day from 2006-2023 across all grid cells (10 km) in the contiguous U.S. For non-smoke days, we used the non-smoke models to predict O_3 concentrations on those days across the contiguous U.S. These predictions on non-smoke days use feature values observed on that day, e.g., meteorology and precursor concentration, and are thus designed to represent the actual O_3 concentration on those days. For smoke days, we used our ML models to create three sets of predictions (Figure 1):

- *Predicted total O_3* $= f_S(M, P, G, F)$, where f_S represents the smoke ML models, and M,P,G,F represent the input features of meteorology variables (M), precursor variables (P), geographical variables (G), and fire-related variables (F). *Predicted total O_3* is predicted from the smoke model, using meteorological and precursor variables observed on the corresponding smoke day. *Predicted total O_3* thus estimates the total O_3 concentration from both smoke and non-smoke sources on smoke days.

- *Counterfactual O_3* $= f_{NS}(M, \overline{P_{NS}}, G)$, where f_{NS} represents the non-smoke ML models, and $\overline{P_{NS}}$ represents the values of precursor variables averaged over non-smoke days in the same month with 3-year windows. Note that *Counterfactual O_3* is predicted from the non-smoke models using meteorological variables observed on the corresponding smoke day and average precursor values on non-smoke days. *Counterfactual O_3* thus estimates the counterfactual non-smoke O_3 concentration on smoke days given the observed meteorological conditions.

- *Non-Smoke met O_3* $= f_{NS}(\overline{M}, \overline{P_{NS}}, G)$, where f_{NS} represents the non-smoke ML models, $\overline{M}$ represents the average meteorological conditions over non-smoke days, and $\overline{P_{NS}}$ represents the average precursor variables over non-smoke days. Note that *Non-Smoke met O_3* is predicted from the non-smoke model using average meteorological and precursor variable values on non-smoke days. *Non-Smoke met O_3* thus quantifies the counterfactual non-smoke O_3 concentration on smoke days given the typical non-smoke meteorological conditions for this grid cell. Non-smoke meteorological conditions are defined as the mean values of meteorological variables on all non-smoke days in the same month and the moving 3-year window.

We then used these three sets of predictions on smoke days to estimate the contribution of wildfire smoke to ground-level O_3 concentrations and the contribution of meteorological variability between smoke and non-smoke days on O_3 concentrations. Specifically, we calculated two values for each smoke day:

$$\text{Smoke-driven } O_3 = \textit{Predicted total } O_3 - \textit{Counterfactual } O_3 \tag{1}$$

$$\text{Met-driven } O_3 = \textit{Counterfactual } O_3 - \textit{Non-Smoke met } O_3 \tag{2}$$

Here, *Smoke-driven* O_3 denotes the contribution of wildfire smoke to ground-level O_3 concentrations while controlling for meteorological variability between smoke and non-smoke days. Importantly, *Smoke-driven* O_3 does not include the potential O_3 changes due to meteorological variability across smoke and non-smoke days (e.g., smoke days are hotter). We use *Smoke-driven* O_3 as our main estimate for smoke O_3 concentration. *Met-driven* O_3 quantifies the effects of meteorological variability on O_3 concentrations, which is not necessarily due to smoke influences. We retain all values of *Smoke-driven* O_3 and *Met-driven* O_3, whether positive or negative, in all calculations. *Smoke-driven* O_3 are assumed to be zero on non-smoke days.

Our final dataset thus includes daily grid-cell estimates across 95,549 grid cells from 2006-2023 (grid cells with water coverage >50% are excluded). As we construct two versions of the smoke model, one with and one without interpolated O_3 concentrations, we generate two sets of predicted total O_3 concentrations and estimated *Smoke-driven* O_3 for all smoke days. We do not construct non-smoke models with interpolated O_3 concentrations because our non-smoke models are used for quantifying the contribution of meteorological variability. As a result, our final model only includes one set of predicted total O_3 concentrations for all non-smoke days, and one set of predictions for *Met-driven* O_3 on smoke days.

Impacts on AQI and extreme O_3

We calculated daily AQI values for each 10 km grid cell from estimated MDA8 O_3 and $PM_{2.5}$ concentrations, following the EPA reporting guidance (*45*). We defined the reported AQI as the maximum of the $PM_{2.5}$ and O_3 sub-indices, and thus ignored the potential contributions from other pollutants. We used the breakpoints from the 2026 EPA AQI guidelines and retrospectively applied them back to 2006. Total $PM_{2.5}$ was constructed as the sum of daily smoke $PM_{2.5}$ from Childs et al. (*56*) and a monthly non-smoke baseline, obtained by subtracting monthly mean smoke $PM_{2.5}$ from satellite-derived total $PM_{2.5}$ (*74*). We classified a grid-day as smoke-driven when its AQI category based on total concentrations was higher than the category based on counterfactual non-smoke concentrations of both pollutants. Among smoke-driven AQI days, we attributed the AQI category to O_3 only, $PM_{2.5}$ only, or both, according to which sub-index reached the reported category. As the AQI is defined as the maximum across pollutants, at least one sub-index always reaches it, so these three groups are mutually exclusive and exhaustive. All results are reported as person-days under each AQI category. Because the calculated monthly non-smoke $PM_{2.5}$ baseline omits day-to-day variation in background $PM_{2.5}$ and smoke days often correspond to higher non-smoke $PM_{2.5}$ (*56*), our approach likely overstates the share of smoke-driven days attributable to $PM_{2.5}$ alone and understates the share attributable to O_3 alone.

We further quantified how wildfire smoke alters the duration and intensity of short-term extreme O_3 episodes. We identified extreme O_3 episodes using a centered rolling mean of daily O_3 concentrations in the observed smoke scenario (i.e., using estimated total smoke O_3 concentrations). In the primary analysis, we defined an episode as at least two consecutive days with a 3-day mean O_3 concentration greater than a threshold of 60 ppb. The episode duration was defined as the union of the corresponding rolling windows, and each episode was required to contain at least one smoke day. To characterize the intensity of extreme O_3, we calculated the mean and peak daily O_3 concentrations within the episode. We then calculated the duration, mean, and peak daily O_3 concentration ignoring the smoke influences for each episode. The effects of wildfire smoke were quantified as the differences between the paired smoke and non-smoke scenarios in duration, mean O_3, and peak O_3. We also assessed the robustness of these estimates using alternative thresholds of 55, 65, and 70 ppb (Figure S15).

Acknowledgments

M.Q. acknowledged the support from Minghua Zhang faculty career catalyst award from Stony Brook University. X.J. acknowledged the support from NOAA Climate Program Office's Atmospheric Chemistry, Carbon Cycle, and Climate program (grant number: NA22OAR4310199). K.C. was supported by the National Heart, Lung, and Blood Institute of the National Institutes of Health (R01HL169171). Role of the Funder/Sponsor: The funder had no role in the design and conduct of the study; collection, management, analysis, and interpretation of the data; preparation, review, or approval of the manuscript; and decision to submit the manuscript for publication.

Author contributions

M.Q. designed the research. Y.L. led the development of machine learning models, with inputs from M.C., M.K., X.J., and K.C. M.Q. and Y.L. led the analysis on smoke ozone exposure patterns, with inputs from all co-authors. M.Q. and Y.L. drafted the manuscript with inputs from all co-authors. All authors reviewed and approved the manuscript.

Competing interests

The authors declare no competing interests.

Data and materials availability

Generated daily smoke O_3 data can be downloaded at https://doi.org/10.5281/zenodo.20346286. Replication data and materials to produce the main results and figures of the paper are available at https://github.com/mhqiu/US-smoke-ozone.

References

1. M. Burke *et al.*, The contribution of wildfire to PM2. 5 trends in the USA. *Nature* **622**, 761–766 (2023).

2. D. Zhang *et al.*, Wildland Fires Worsened Population Exposure to PM2. 5 Pollution in the Contiguous United States. *Environmental Science & Technology* **57**, 19990–19998 (2023).

3. D. Jaffe, H. Lee, S. Magzamen, D. L. Goldberg, K. O'Dell, Health and regulatory impacts of PM2. 5 from wildland fires for 2019–2024 in the US. *GeoHealth* **10**, e2025GH001576 (2026).

4. T. Benmarhnia *et al.*, Wildfire smoke PM2. 5 as a growing source of emission and the challenges for current air quality regulations. *Environment International*, 110305 (2026).

5. C. F. Gould *et al.*, Health effects of wildfire smoke exposure. *Annual Review of Medicine* **75**, 277–292 (2024).

6. C. E. Reid *et al.*, Critical review of health impacts of wildfire smoke exposure. *Environmental Health Perspectives* **124**, 1334–1343 (2016).

7. S. Heft-Neal *et al.*, Emergency department visits respond nonlinearly to wildfire smoke. *Proceedings of the National Academy of Sciences* **120**, e2302409120 (2023).

8. A. Heaney *et al.*, Impacts of fine particulate matter from wildfire smoke on respiratory and cardiovascular health in California. *GeoHealth* **6**, e2021GH000578 (2022).

9. M. D. Yazdi, N. Sasaki, M. Qiu, G. Huang, P. E. Sheffield, The effect of wildfire air pollution on local hospital admissions in New York. *Environmental Research Communications* **8**, 051014 (2026).

10. Y. S. Jung *et al.*, Fine Particulate Matter From 2020 California Wildfires and Mental Health–Related Emergency Department Visits. *JAMA Network Open* **8**, e253326 (2025).

11. Y. Ma *et al.*, Long-term exposure to wildland fire smoke PM2. 5 and mortality in the contiguous United States. *Proceedings of the National Academy of Sciences* **121**, e2403960121 (2024).

12. L. Schwarz *et al.*, Long-term exposure to wildfire smoke and mortality: Heterogeneous effects by exposure metric and across subpopulations. *Proceedings of the National Academy of Sciences* **122**, e2509173122 (2025).

13. M. Zhang *et al.*, Wildfire smoke $PM_{2.5}$ and mortality rate in the contiguous United States: A causal modeling study. *Science Advances* **12**, eadw5890 (2026).

14. M. Qiu *et al.*, Wildfire smoke exposure and mortality burden in the USA under climate change. *Nature* **647**, 935–943 (2025).

15. W. Deng *et al.*, Fires reverse progress toward ozone air quality standards in the United States. *Science* **392**, 1088–1092 (2026).

16. M. L. Childs *et al.*, Daily Local-Level Estimates of Ambient Wildfire Smoke PM2. 5 for the Contiguous US. *Environmental Science & Technology* **56**, 13607–13621 (2022).

17. R. Aguilera *et al.*, A novel ensemble-based statistical approach to estimate daily wildfire-specific PM2. 5 in California (2006–2020). *Environment International* **171**, 107719 (2023).

18. Y. Hu *et al.*, Global high-resolution fire-sourced $PM_{2.5}$ concentrations for 2000–2023. *Earth System Science Data* **17**, 3741–3756 (2025).

19. A. Orr *et al.*, A State of the Science Review of Wildfire-Specific Fine Particulate Matter Data Sources, Methods, and Models. *Environmental Health Perspectives* **133**, 066001 (2025).

20. D. A. Jaffe *et al.*, Wildfire and prescribed burning impacts on air quality in the United States. *Journal of the Air & Waste Management Association* **70**, 583–615 (2020).

21. D. A. Jaffe, N. L. Wigder, Ozone production from wildfires: A critical review. *Atmospheric Environment* **51**, 1–10 (2012).

22. Y. Li, X. Jin, M. Kelp, H. Z. Sun, M. Qiu, Growing impacts of fire smoke on ozone pollution and associated mortality burden in the United States. *Science Advances* **12**, eaec2903 (2026).

23. X. Jin, Q. Zhu, R. C. Cohen, Direct estimates of biomass burning NO x emissions and lifetimes using daily observations from TROPOMI. *Atmospheric Chemistry and Physics* **21**, 15569–15587 (2021).

24. X. Jin, A. M. Fiore, R. C. Cohen, Space-based observations of ozone precursors within California wildfire plumes and the impacts on ozone-NO x-VOC chemistry. *Environmental Science & Technology* **57**, 14648–14660 (2023).

25. S. Liu, D. A. Jaffe, Surface Atmospheric Formaldehyde Trends in the US Driven by Temperature-Dependent Biogenic Precursor Emissions and Influenced by Wildfires. *ACS ES&T Air* **3**, 1167–1175 (2026).

26. M. Lin, L. W. Horowitz, L. Hu, W. Permar, Reactive Nitrogen Partitioning Enhances the Contribution of Canadian Wildfire Plumes to US Ozone Air Quality. *Geophysical Research Letters* **51** (2024).

27. O. R. Cooper *et al.*, Early season 2023 wildfires generated record-breaking surface ozone anomalies across the US Upper Midwest. *Geophysical Research Letters* **51**, e2024GL111481 (2024).

28. J. Shen, R. C. Cohen, G. M. Wolfe, X. Jin, Impacts of wildfire smoke aerosols on near-surface ozone photochemistry. *Atmospheric Chemistry and Physics* **25**, 8701–8718 (2025).

29. X. Jiang, C. Wiedinmyer, A. G. Carlton, Aerosols from fires: An examination of the effects on ozone photochemistry in the Western United States. *Environmental Science & Technology* **46**, 11878–11886 (2012).

30. M. Lin, L. W. Horowitz, R. Payton, A. M. Fiore, G. Tonnesen, US surface ozone trends and extremes from 1980 to 2014: quantifying the roles of rising Asian emissions, domestic controls, wildfires, and climate. *Atmospheric Chemistry and Physics* **17**, 2943–2970 (2017).

31. L. Xu *et al.*, Ozone chemistry in western US wildfire plumes. *Science Advances* **7**, eabl3648 (2021).

32. J. O. Palmo *et al.*, Investigating fire-induced ozone production from local to global scales. *Atmospheric Chemistry and Physics* **25**, 17107–17124 (2025).

33. S. J. Brey, E. V. Fischer, Smoke in the city: How often and where does smoke impact summertime ozone in the United States? *Environmental Science & Technology* **50**, 1288–1294 (2016).

34. H. Lee, D. A. Jaffe, Wildfire impacts on O3 in the continental United States using PM2. 5 and a generalized additive model (2018–2023). *Environmental Science & Technology* **58**, 14764–14774 (2024).

35. H. Lee, D. A. Jaffe, Impact of wildfires on O3 and air quality across the United States for 2019–2024 using generalized additive models. *Journal of Geophysical Research: Atmospheres* **130**, e2025JD044088 (2025).

36. W. S. Chace *et al.*, The Influence of Aged Smoke on Urban Ozone: Aircraft Measurements in Chicago during the 2023 Canadian Wildfires. (2026).

37. R. Aguilera, T. Benmarhnia, Effects of Multiple Wildfire Smoke Pollutants ($PM_{2.5}$, PM_{10}, and Ozone) on Respiratory and Cardiovascular Hospitalizations in California (2006–2019). *GeoHealth* (2025).

38. L. Jin *et al.*, Characterizing emissions, chemistry, and health impacts of aged wildfire smoke in a western US city. *EGUsphere*, Preprint (2026).

39. R. Xu *et al.*, Global population exposure to landscape fire air pollution from 2000 to 2019. *Nature* **621**, 521–529 (2023).

40. K. O'Dell, B. Ford, E. V. Fischer, J. R. Pierce, Contribution of wildland-fire smoke to US PM2. 5 and its influence on recent trends. *Environmental Science & Technology* **53**, 1797–1804 (2019).

41. S. N. Koplitz, C. G. Nolte, G. A. Pouliot, J. M. Vukovich, J. Beidler, Influence of uncertainties in burned area estimates on modeled wildland fire $PM_{2.5}$ and ozone pollution in the contiguous U.S. *Atmospheric Environment* **191**, 328–339 (2018).

42. T. S. Carter *et al.*, How emissions uncertainty influences the distribution and radiative impacts of smoke from fires in North America. *Atmospheric Chemistry and Physics* **20**, 2073–2097 (2020).

43. L. Jin *et al.*, Ozone photochemistry in fresh biomass burning smoke over the United States. *Science Advances* **12**, eads2157 (2026).

44. M. Qiu *et al.*, Evaluating Chemical Transport and Machine Learning Models for Wildfire Smoke PM2. 5: Implications for Assessment of Health Impacts. *Environmental Science & Technology* **58**, 22880–22893 (2024).

45. U.S. Environmental Protection Agency, "Technical Assistance Document for the Reporting of Daily Air Quality – the Air Quality Index (AQI)", tech. rep. EPA-403/B-26-003 (U.S. Environmental Protection Agency, Office of Air Quality Planning and Standards, Air Quality Assessment Division, Research Triangle Park, NC, May 2026).

46. J. A. Casey *et al.*, Measuring long-term exposure to wildfire PM2.5 in California: Time-varying inequities in environmental burden. *Proceedings of the National Academy of Sciences* **121**, e2306729121 (2024).

47. L. R. Dennin, D. Nock, N. Z. Muller, M. Akindele, P. J. Adams, Socially vulnerable communities face disproportionate exposure and susceptibility to U.S. wildfire and prescribed burn smoke. *Communications Earth & Environment* **6**, 190 (2025).

48. W. J. Requia *et al.*, An ensemble learning approach for estimating high spatiotemporal resolution of ground-level ozone in the contiguous United States. *Environmental science & technology* **54**, 11037–11047 (2020).

49. X. Huang *et al.*, Smoke-weather interaction affects extreme wildfires in diverse coastal regions. *Science* **379**, 457–461 (2023).

50. G. A. Kelesidis *et al.*, Radiative cooling in New York/New Jersey metropolitan areas by wildfire particulate matter emitted from the Canadian wildfires of 2023. *Communications Earth & Environment* **6**, 304 (2025).

51. C. Liu *et al.*, Interactive effects of ambient fine particulate matter and ozone on daily mortality in 372 cities: two stage time series analysis. *bmj* **383** (2023).

52. N. Siddika *et al.*, Synergistic effects of prenatal exposure to fine particulate matter (PM2. 5) and ozone (O3) on the risk of preterm birth: A population-based cohort study. *Environmental research* **176**, 108549 (2019).

53. T. Liu *et al.*, Is the smoke aloft? Caveats regarding the use of the Hazard Mapping System (HMS) smoke product as a proxy for surface smoke presence across the United States. *International Journal of Wildland Fire* **33** (2024).

54. L Shen, L. Mickley, A. Tai, Influence of synoptic patterns on surface ozone variability over the eastern United States from 1980 to 2012. *Atmospheric Chemistry and Physics* **15**, 10925–10938 (2015).

55. D. A. Jaffe *et al.*, Scientific assessment of background ozone over the U.S.: Implications for air quality management. *Elementa: Science of the Anthropocene* **6**, 56 (2018).

56. M. Childs *et al.*, Growing wildfire-derived PM2. 5 across the contiguous US and implications for air quality regulation. (2024).

57. A. Krupnick, N. Richardson, M. Wibbenmeyer, Wildfire Smoke, the Clean Air Act, and the Exceptional Events Rule: Implications and Policy Alternatives. *Environmental Science & Technology* **59**, 2917–2927 (2025).

58. L. Emberson, Effects of ozone on agriculture, forests and grasslands. *Philosophical Transactions of the Royal Society A* **378**, 20190327 (2020).

59. M. Qiu *et al.*, Valuing wildfire smoke–related mortality benefits from climate mitigation. *Proceedings of the National Academy of Sciences* **123**, e2533772123 (2026).

60. Y. Xie *et al.*, Tripling of western US particulate pollution from wildfires in a warming climate. *Proceedings of the National Academy of Sciences* **119**, e2111372119 (2022).

61. U.S EPA, "Overview of Ozone (O3) Air Quality in the United States", tech. rep.

62. W Schroeder *et al.*, Validation analyses of an operational fire monitoring product: The Hazard Mapping System. *International Journal of Remote Sensing* **29**, 6059–6066 (2008).

63. M. Ruminski, S. Kondragunta, R. Draxler, J. Zeng, presented at the Proceedings of the 15th International Emission Inventory Conference, vol. 15, p. 18.

64. L. Giglio, W. Schroeder, C. O. Justice, The collection 6 MODIS active fire detection algorithm and fire products. *Remote Sensing of Environment* **178**, 31–41 (2016).

65. D. Davies *et al.*, presented at the EARSel Forest Fires SIG Workshop.

66. A. Inness *et al.*, The CAMS reanalysis of atmospheric composition. *Atmospheric Chemistry and Physics* **19**, 3515–3556 (2019).

67. H. Hersbach *et al.*, The ERA5 global reanalysis. *Quarterly Journal of the Royal Meteorological Society* **146**, 1999–2049 (2020).

68. J. Muñoz Sabater *et al.*, ERA5-Land: a state-of-the-art global reanalysis dataset for land applications. *Earth System Science Data* **13**, 4349–4383 (2021).

69. G. Amatulli *et al.*, A suite of global, cross-scale topographic variables for environmental and biodiversity modeling. *Scientific Data* **5**, 1–15 (2018).

70. D. Sulla-Menashe, M. A. Friedl, *et al.*, User guide to collection 6 MODIS land cover (MCD12Q1 and MCD12C1) product. *Usgs: Reston, Va, Usa* **1**, 18 (2018).

71. J. Voorheis *et al.*, "The Privacy-Protected Gridded Environmental Impacts Frame", Working Papers 24-74 (Center for Economic Studies, U.S. Census Bureau, Dec. 2024).

72. T. Chen, C. Guestrin, presented at the Proceedings of the 22nd ACM SIGKDD International Conference on Knowledge Discovery and Data Mining, pp. 785–794.

73. L. Prokhorenkova, G. Gusev, A. Vorobev, A. V. Dorogush, A. Gulin, CatBoost: unbiased boosting with categorical features. *Advances in neural information processing systems* **31** (2018).

74. A. van Donkelaar *et al.*, North American Fine Particulate Matter Chemical Composition for 2000–2022 from Satellites, Models, and Monitors: The Changing Contribution of Wildfires. *ACS ES&T Air* **1**, 1589–1600 (2024).

75. S. M. Lundberg, S.-I. Lee, A unified approach to interpreting model predictions. *Advances in neural information processing systems* **30** (2017).

Table S1: Feature inputs of machine learning models. All variables are at daily resolution, except for population, elevation, and land cover (which are time-invariant). All variables are regridded to 10 km for model training and predictions.

Type	**Feature**	**Resolution**	**Source**
Meteorology	Temperature (Min, Max, Mean) Dewpoint (Min, Max, Mean) Surface pressure Wind (U, V, speed, direction) Precipitation Soil moisture LAI (High and Low vegetation)	9 km	ERA5-Land (*68*)
	Mean sea level pressure UV radiation Total cloud cover Total column ozone Boundary layer height	25 km	ERA5 (*67*)
O_3 Precursor	NO_2 (at 1000 hPa level) Formaldehyde (at 1000 hPa level)	75 km	CAMS (EAC4) (*66*)
Geography	Land cover (resampled to 10 categories: Water, Forest, Shrub, Savanna, Grass, Wetland, Crop, Urban, Ice, Barren) Distance to water	5 km	MCD12C1 (MODIS)
	Elevation	1 km	EarthEnv (*69*)
	Population	1 km	Gridded EIF (*71*)
Fire	Fire radiative power (FRP) Distance to fire	points	FIRMS (MODIS C6.1)
	Smoke $PM_{2.5}$	10 km	Childs et al. (*56*)
Others	Day of the year	–	–

Table S2: Out-of-sample performance metrics of smoke and non-smoke O_3 models, reported based on spatial cross-validation at 75 km. Within R^2 is calculated from linear regressions that include station and month fixed effects, thus capturing the models' ability to capture spatio-temporal variability beyond seasonality and time-invariant location differences. Warm season is defined as April to September.

Model group	**Learner**	R^2	**Within** R^2	**RMSE (ppb)**	**MAE (ppb)**
Non-smoke (all-year)	XGBoost	0.73	0.58	7.23	5.42
	CatBoost	0.73	0.57	7.34	5.53
	Neural Network	0.69	0.52	7.74	5.85
	Ensemble	0.73	0.57	7.28	5.47
Non-smoke (warm-season)	XGBoost	0.69	0.56	7.94	5.99
	CatBoost	0.69	0.56	8.05	6.13
	Neural Network	0.65	0.51	8.46	6.47
	Ensemble	0.68	0.56	7.98	6.05
Smoke (no interpolation)	XGBoost	0.74	0.65	7.33	5.41
	CatBoost	0.72	0.62	7.75	5.83
	Neural Network	0.66	0.54	8.23	6.25
	Ensemble	0.73	0.64	7.39	5.50
Smoke (with interpolation)	XGBoost	0.86	0.81	5.61	3.96
	CatBoost	0.86	0.81	5.58	3.93
	Neural Network	0.85	0.80	5.79	4.11
	Ensemble	0.85	0.81	5.73	4.07

Table S3: Population-weighted annual 4th maximum MDA8 O_3 concentrations by state (unit: ppb). Three separate periods, 2006-2023, 2006-2008, and 2021-2023, are shown in the table.

	Non-smoke O_3			**Total O_3**			**Smoke Contribution**		
State	2006–2023	2006–2008	2021–2023	2006–2023	2006–2008	2021–2023	2006–2023	2006–2008	2021–2023
contiguous U.S.	63.3	67.7	60.1	65.9	69.8	65.0	2.58	2.12	4.90
Alabama	62.8	69.9	59.0	64.1	71.3	61.6	1.32	1.41	2.59
Arizona	67.5	68.6	67.5	69.0	68.6	71.3	1.42	0.06	3.80
Arkansas	62.1	67.5	60.7	63.6	68.6	63.1	1.50	1.13	2.43
California	67.6	70.7	65.7	69.8	72.3	69.0	2.21	1.59	3.28
Colorado	64.0	65.1	63.6	67.0	66.5	69.2	2.97	1.47	5.62
Connecticut	66.3	73.5	58.4	70.1	76.0	66.9	3.81	2.53	8.46
Delaware	65.8	72.8	58.4	68.4	74.3	63.6	2.61	1.49	5.17
Florida	58.6	60.9	55.5	60.2	64.3	57.9	1.61	3.47	2.40
Georgia	65.0	73.7	60.4	66.6	75.7	63.5	1.61	2.01	3.05
Idaho	59.1	60.1	58.7	62.3	62.1	63.7	3.17	1.97	5.03
Illinois	63.7	67.4	62.2	67.5	68.7	70.5	3.78	1.27	8.30
Indiana	64.1	69.0	61.5	67.0	71.1	67.6	2.91	2.15	6.06
Iowa	58.9	60.5	59.1	61.2	61.6	63.9	2.29	1.08	4.75
Kansas	61.6	63.3	60.8	63.6	64.4	64.8	2.03	1.17	4.00
Kentucky	64.3	69.6	61.8	65.9	71.4	64.2	1.61	1.75	2.36
Louisiana	61.6	66.5	57.7	63.4	67.7	61.7	1.80	1.28	3.97
Maine	53.5	55.9	50.4	55.8	59.1	54.9	2.29	3.17	4.52
Maryland	67.1	75.4	59.2	69.3	76.9	64.2	2.14	1.52	4.99
Massachusetts	60.3	66.0	53.6	64.2	69.9	62.0	3.89	3.97	8.34
Michigan	61.5	65.0	58.5	66.0	69.6	66.9	4.56	4.55	8.42
Minnesota	57.5	59.4	56.5	60.2	61.1	62.4	2.69	1.61	5.84
Mississippi	60.5	65.5	57.5	61.8	66.7	60.4	1.35	1.15	2.91
Missouri	63.0	67.2	62.7	65.3	69.8	65.8	2.29	2.63	3.17
Montana	54.7	55.8	54.2	57.9	58.5	59.8	3.24	2.72	5.62
Nebraska	57.5	58.1	57.9	59.4	58.7	62.2	1.91	0.60	4.27
Nevada	66.7	68.5	65.5	68.8	70.6	68.7	2.14	2.10	3.18
New Hampshire	58.6	63.1	53.5	61.2	66.7	59.3	2.67	3.58	5.85

...

Table S3

State	Non-smoke O_3			Total O_3			Smoke Contribution		
	2006–2023	2006–2008	2021–2023	2006–2023	2006–2008	2021–2023	2006–2023	2006–2008	2021–2023
New Jersey	68.3	76.8	59.3	71.5	79.1	66.7	3.25	2.34	7.38
New Mexico	61.5	61.5	61.8	63.6	62.5	66.2	2.10	0.96	4.39
New York	63.4	69.1	57.4	67.0	71.6	65.4	3.57	2.51	8.01
North Carolina	62.4	67.9	59.1	64.2	70.7	62.4	1.86	2.82	3.33
North Dakota	53.7	54.2	53.8	56.8	55.3	59.3	3.04	1.15	5.50
Ohio	64.8	70.4	61.5	67.4	73.2	65.8	2.63	2.75	4.33
Oklahoma	64.9	67.1	64.4	66.9	68.6	67.3	2.01	1.50	2.82
Oregon	53.6	55.6	52.3	58.3	58.8	58.9	4.66	3.20	6.60
Pennsylvania	65.4	72.5	60.2	67.5	74.3	64.0	2.06	1.83	3.86
Rhode Island	63.5	69.6	56.8	67.9	73.0	64.8	4.45	3.40	8.09
South Carolina	61.6	66.8	58.7	62.9	68.7	61.4	1.27	1.97	2.71
South Dakota	55.5	55.6	56.1	58.7	56.8	62.7	3.19	1.25	6.65
Tennessee	64.1	70.6	61.0	65.6	72.3	64.0	1.51	1.75	3.01
Texas	64.4	68.3	61.0	67.6	70.2	67.6	3.27	1.95	6.55
Utah	65.7	67.9	64.4	68.7	70.9	69.8	3.00	2.96	5.42
Vermont	55.7	58.7	53.9	57.0	60.1	57.0	1.27	1.45	3.09
Virginia	63.1	69.4	57.8	64.8	71.3	61.5	1.71	1.87	3.67
Washington	51.5	52.4	51.1	54.8	54.1	56.0	3.28	1.77	4.86
West Virginia	61.5	66.7	58.7	62.6	67.8	60.5	1.01	1.15	1.81
Wisconsin	60.1	62.9	58.6	64.3	64.7	67.2	4.19	1.84	8.60
Wyoming	57.2	58.1	57.0	60.0	59.6	61.6	2.71	1.55	4.58

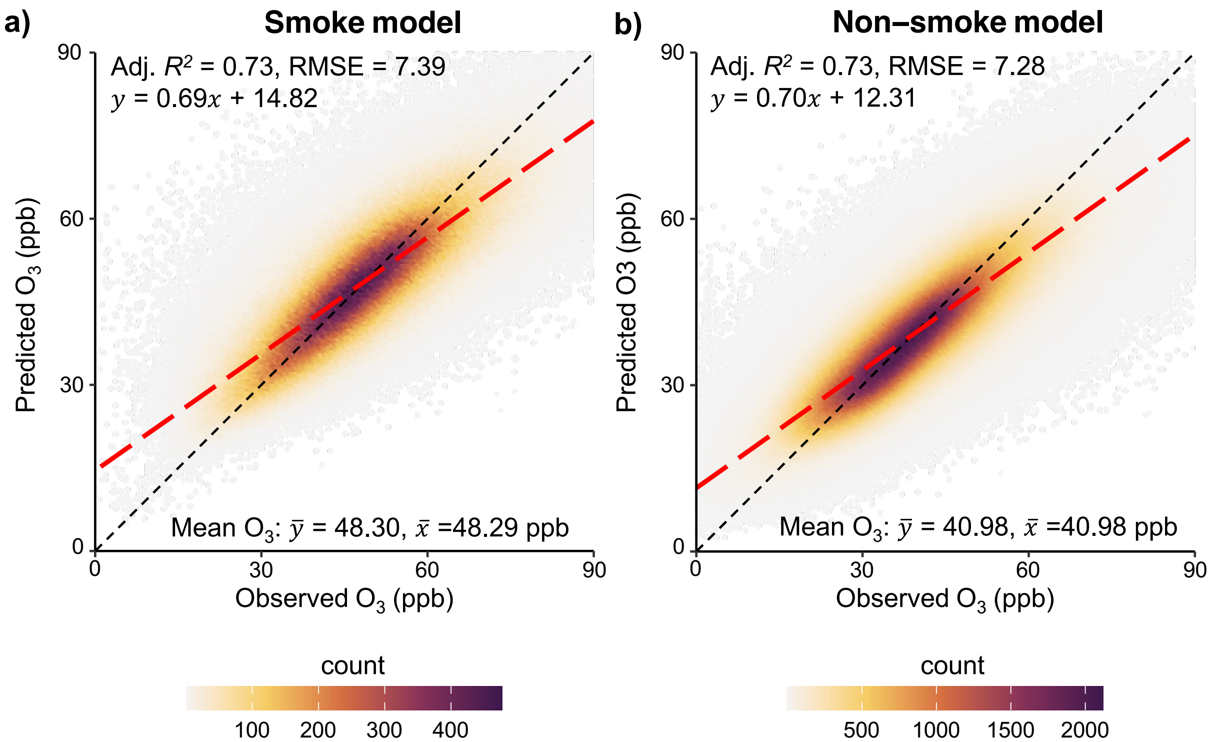

Figure S1: **Out-of-sample performance of ML models.** The figure shows the out-of-sample performance of our smoke and non-smoke ML models in predicting O_3 on smoke days and non-smoke days. x-axis shows the observed daily MDA8 O_3 concentration, and y-axis shows the predicted concentrations. The mean of observed and predicted O_3 concentrations, best linear fits (red line), R^2, and root mean squared error (RMSE) are shown in the figure. 1:1 line is shown in dashed black.

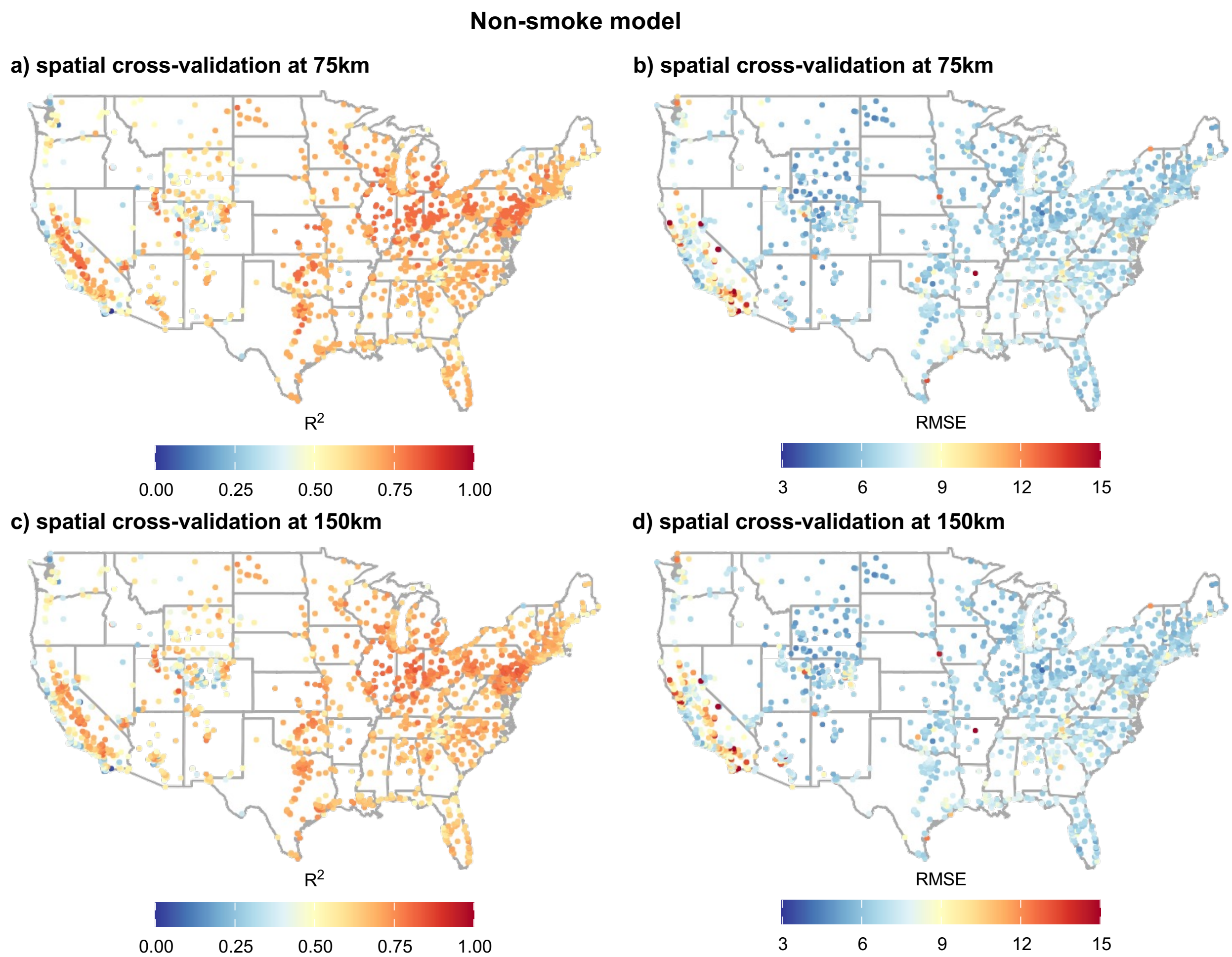

Figure S2: **Model performance of non-smoke ML models.** The figure shows the out-of-sample performance of our non-smoke ML models in predicting O_3 on non-smoke days at each monitoring station. R^2 and root mean squared error (RMSE) are shown in the figure. Results are shown for two spatial cross-validation splits, with the split defined as 75km (a, b) or 150km (c, d).

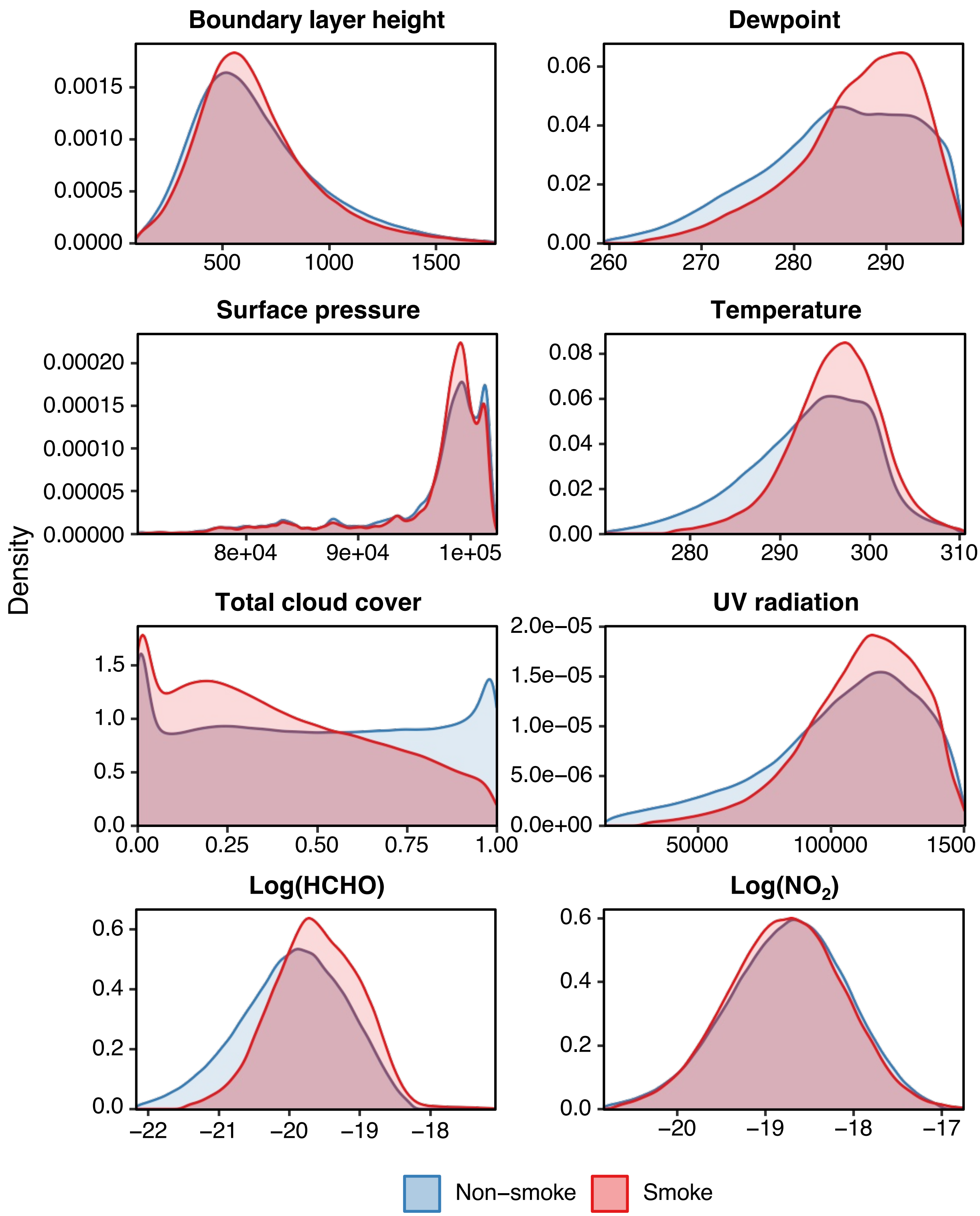

Figure S3: **Distribution of predictors across smoke and non-smoke days.** Density distributions of the eight input predictors used in the ML models, compared between smoke and non-smoke days. Non-smoke days are limited to those in the warm season to be more comparable to smoke days.

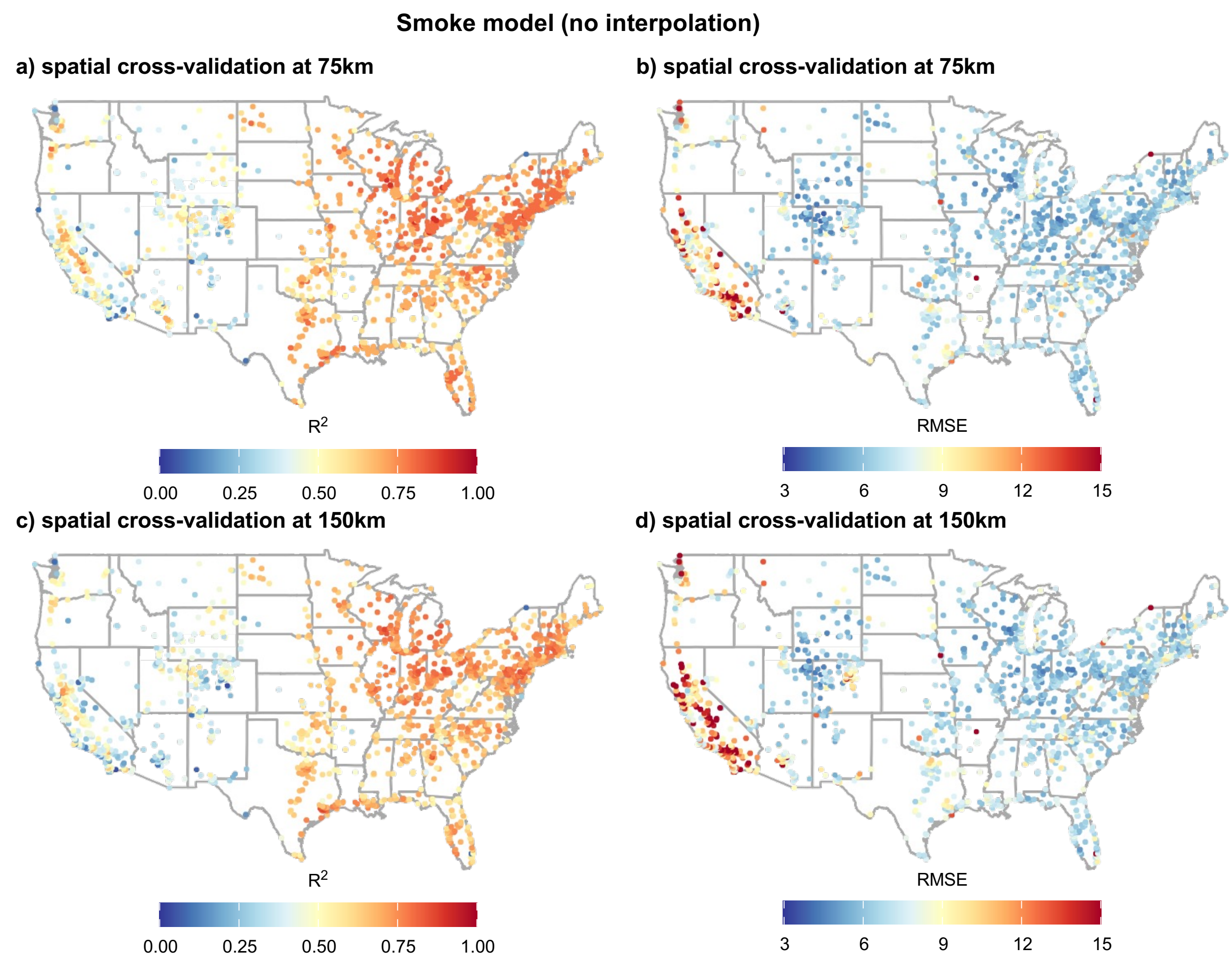

Figure S4: **Model performance of smoke ML models (without using interpolation).** The figure shows the out-of-sample performance of our smoke ML models in predicting O_3 on smoke days at each monitoring station. Importantly, the model does not include interpolated O_3 concentrations from the station data. R^2 and root mean squared error (RMSE) are shown in the figure. Results are shown for two spatial cross-validation splits, with the split defined as 75km (a, b) or 150km (c, d).

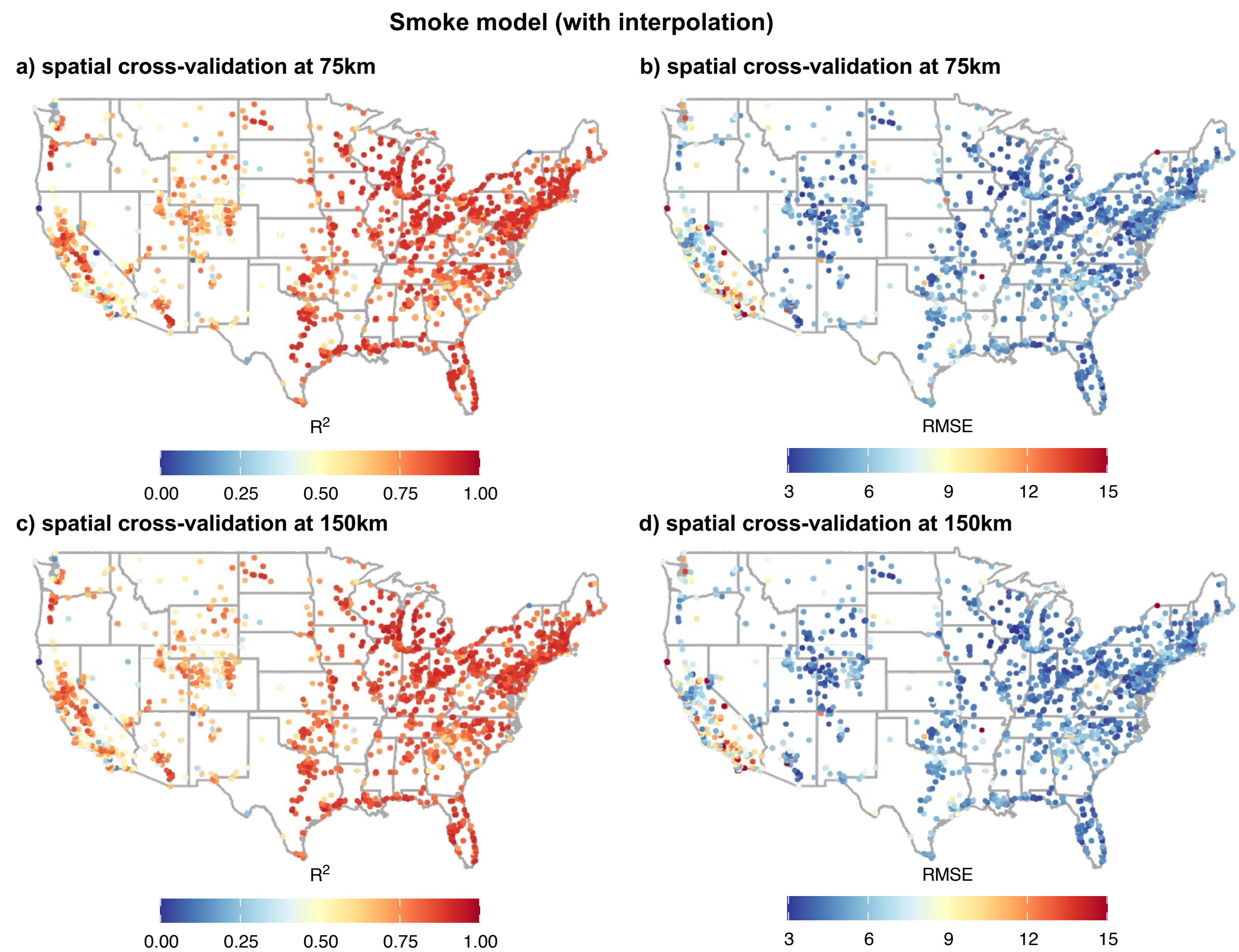

Figure S5: **Model performance of smoke ML models (using interpolation).** The figure shows the out-of-sample performance of our smoke ML models in predicting O_3 on smoke days at each monitoring station. Importantly, the model includes interpolated O_3 concentrations from the station data as a feature. R^2 and root mean squared error (RMSE) are shown in the figure. Results are shown for two spatial cross-validation splits, with the split defined as 75km (a, b) or 150km (c, d).

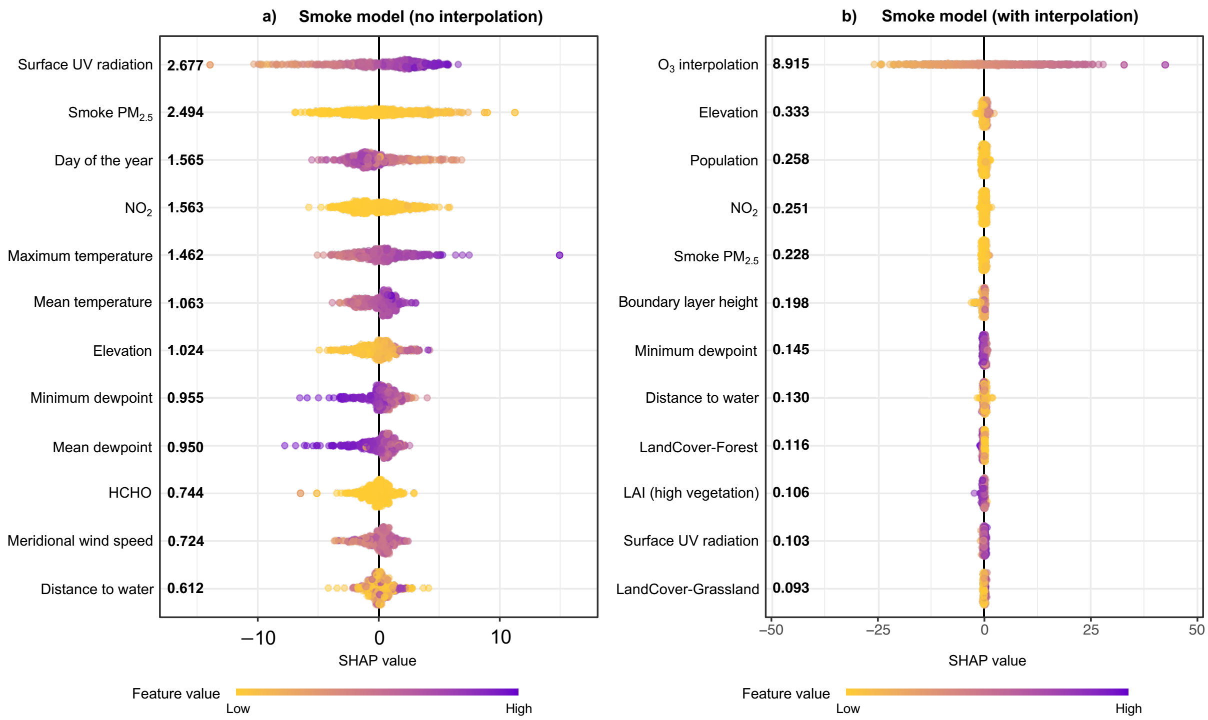

Figure S6: **SHAP value based variable importance for XGBoost smoke models.** Panel a: smoke model (no interpolation). Panel b: smoke model (with interpolation). The SHAP value represents the impact of each feature on the model's prediction relative to the baseline. A larger SHAP value indicates a greater contribution of the feature to model's output, either positively or negatively. Each listed number corresponds to the feature importance, defined as the absolute mean of all SHAP values for a specific feature, reflecting the model's sensitivity to each individual feature. The distribution of points along the horizontal axis shows the range of SHAP values for each feature, with individual points representing the contribution to each observation. The color of the points represents the value of the feature, with low feature values in yellow and high feature values in purple.

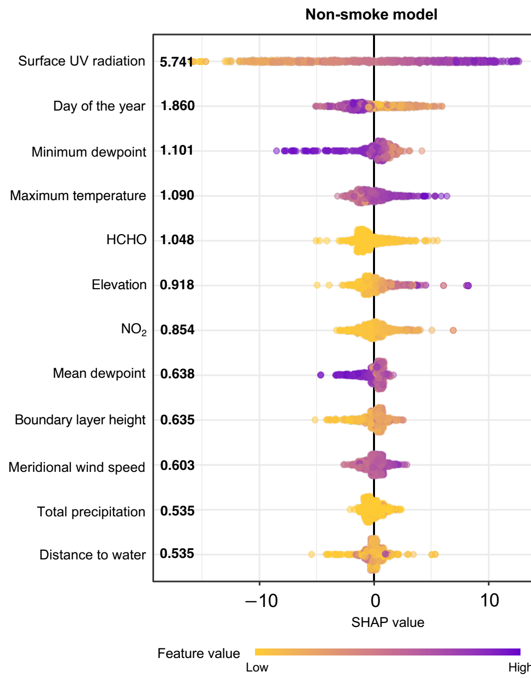

Figure S7: **SHAP value based variable importance for XGBoost non-smoke model.** The SHAP value represents the impact of each feature on the model's prediction relative to the baseline. A larger SHAP value indicates a greater contribution of the feature to model's output, either positively or negatively. Each listed number corresponds to the feature importance, defined as the absolute mean of all SHAP values for a specific feature, reflecting the model's sensitivity to each individual feature. The distribution of points along the horizontal axis shows the range of SHAP values for each feature, with individual points representing the contribution to each observation. The color of the points represents the value of the feature, with low feature values in yellow and high feature values in purple.

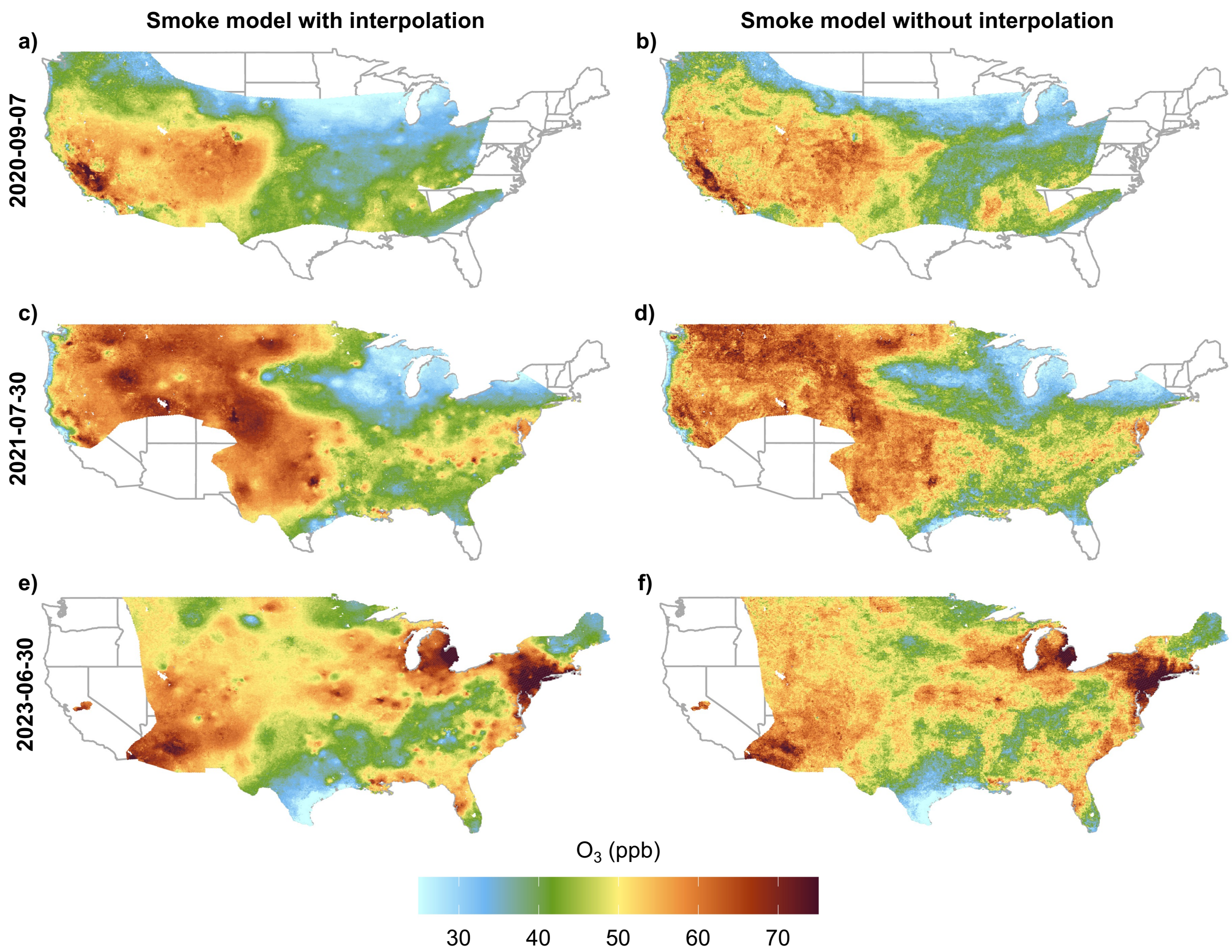

Figure S8: **Spatial patterns of smoke O_3 predictions across interpolation and non-interpolation models (selected smoke days).** The plot shows predictions of O_3 concentrations on three selected smoke days, from the smoke model with interpolation incorporated, and the smoke model without interpolation.

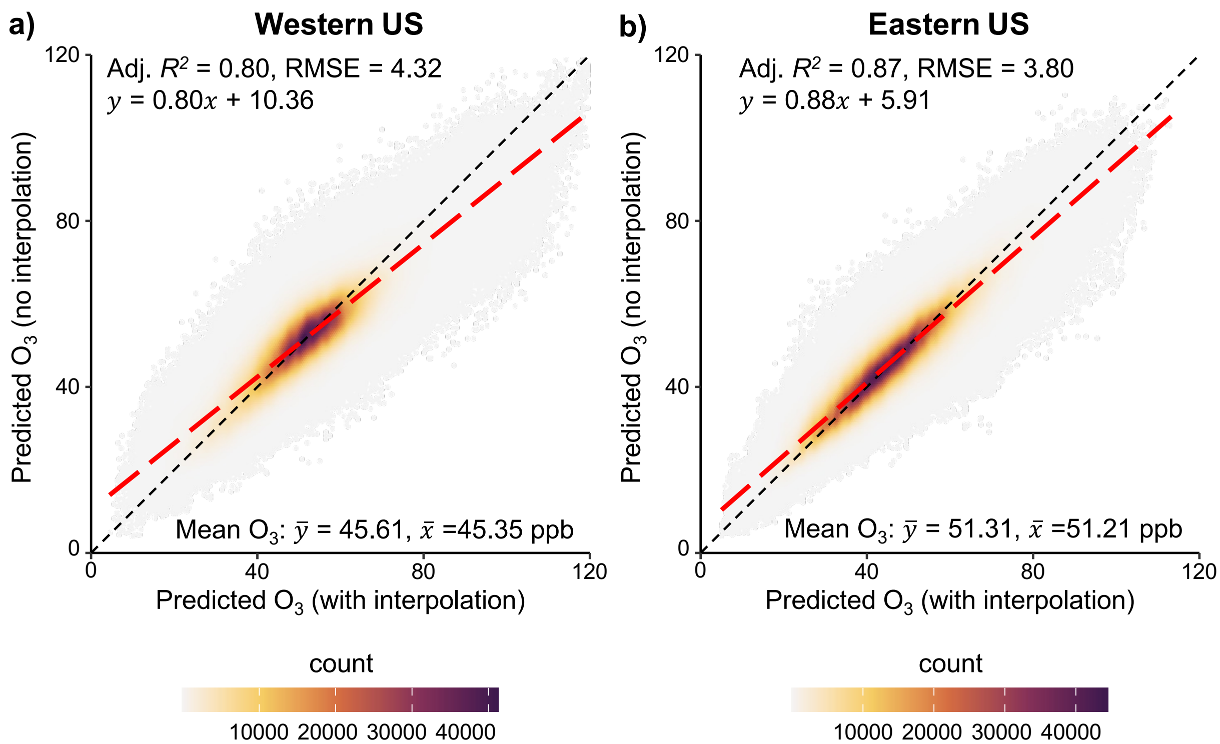

Figure S9: **Comparing smoke O_3 estimated across models with and without interpolation.** The plot shows predictions of O_3 concentrations on smoke days in western and eastern U.S., across models with and without using the interpolations. The y-axis shows the O_3 predictions from ML models without using interpolations (i.e. our main model), and the x-axis shows the O_3 predictions from ML models using interpolations. The western U.S. is defined as locations west of the meridian 100° west.

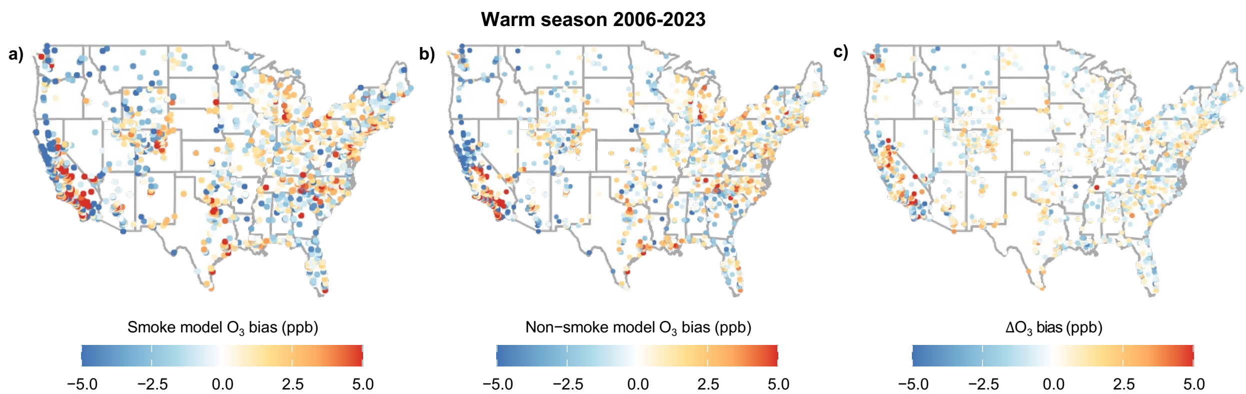

Figure S10: **Prediction bias of O_3 concentrations across monitor locations over the warm season.** The plot shows prediction bias (defined as *predictions - observed*) averaged over the warm season (April to September) from 2006-2023, for smoke days (panel a), non-smoke days (panel b), and their differences (panel c).

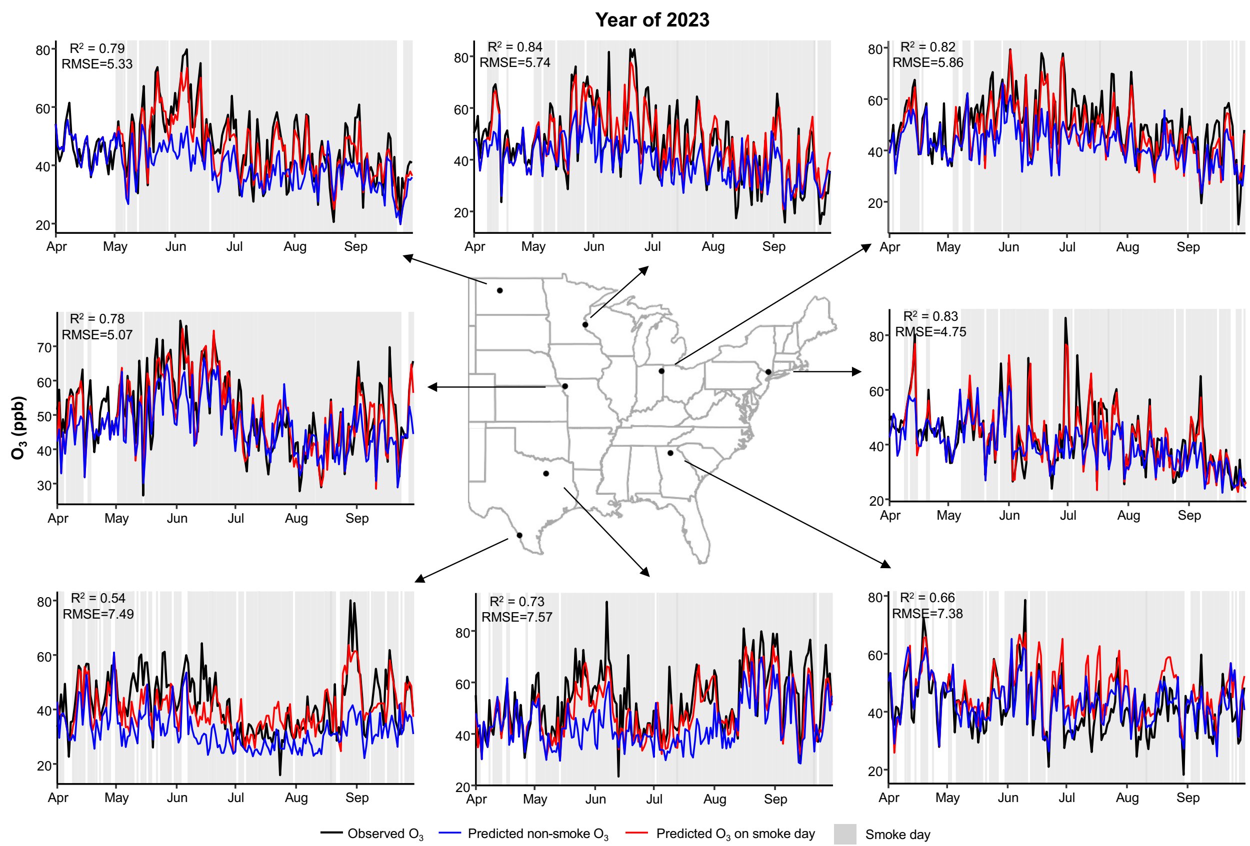

Figure S11: **Observed and predicted daily O_3 concentrations at selected monitoring sites.** Black lines show observed total O_3 concentrations. Blue lines show estimated counterfactual non-smoke O_3 concentrations. Red lines show predicted O_3 concentrations on smoke days from the smoke model. Both blue and red lines are out-of-sample predictions from models trained on datasets that excluded the corresponding site. The plot shows R^2 and RMSE between observed (black) and predicted O_3 concentrations (red line on smoke days + blue line on non-smoke days). Grey shading indicates smoke days identified using HMS smoke polygons.

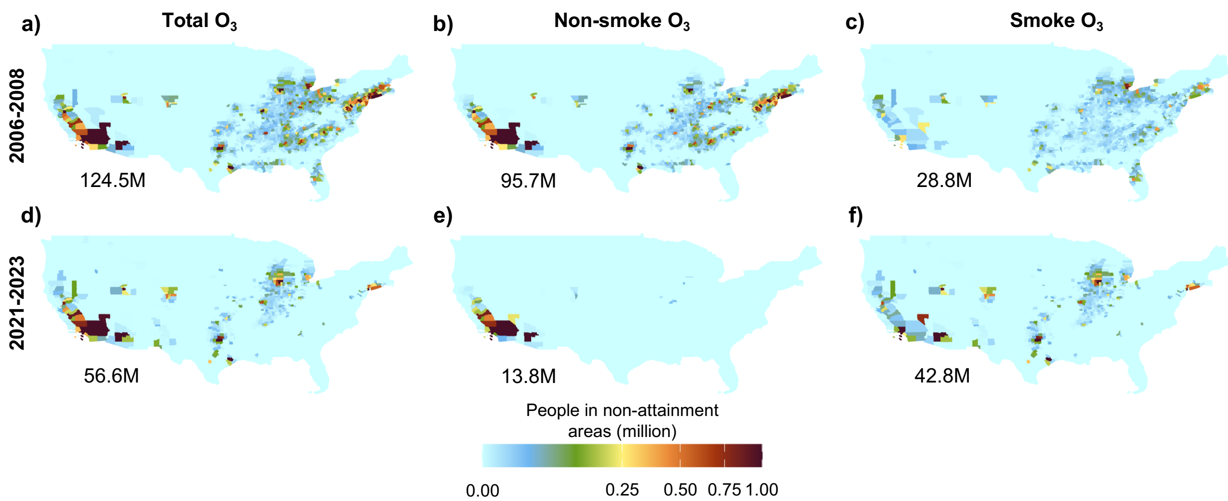

Figure S12: **County-level population in O_3 nonattainment areas.** Nonattainment is determined at the grid-cell level if the 3-year moving average of the annual 4th maximum MDA8 O_3 concentration exceeds 70 ppb. Panels a, b, and c (top row) show results averaged over 2006-2008. Panels d, e, and f (bottom row) show results averaged over 2021-2023. Panels a and d (first column) show nonattainment based on total O_3 concentration (smoke plus non-smoke); panels b and e show nonattainment based on non-smoke O_3; panels c and f show the additional population placed in nonattainment by wildfire smoke (the difference between total and non-smoke O_3). Total population living in nonattainment areas is shown in the bottom-left corner of each panel.

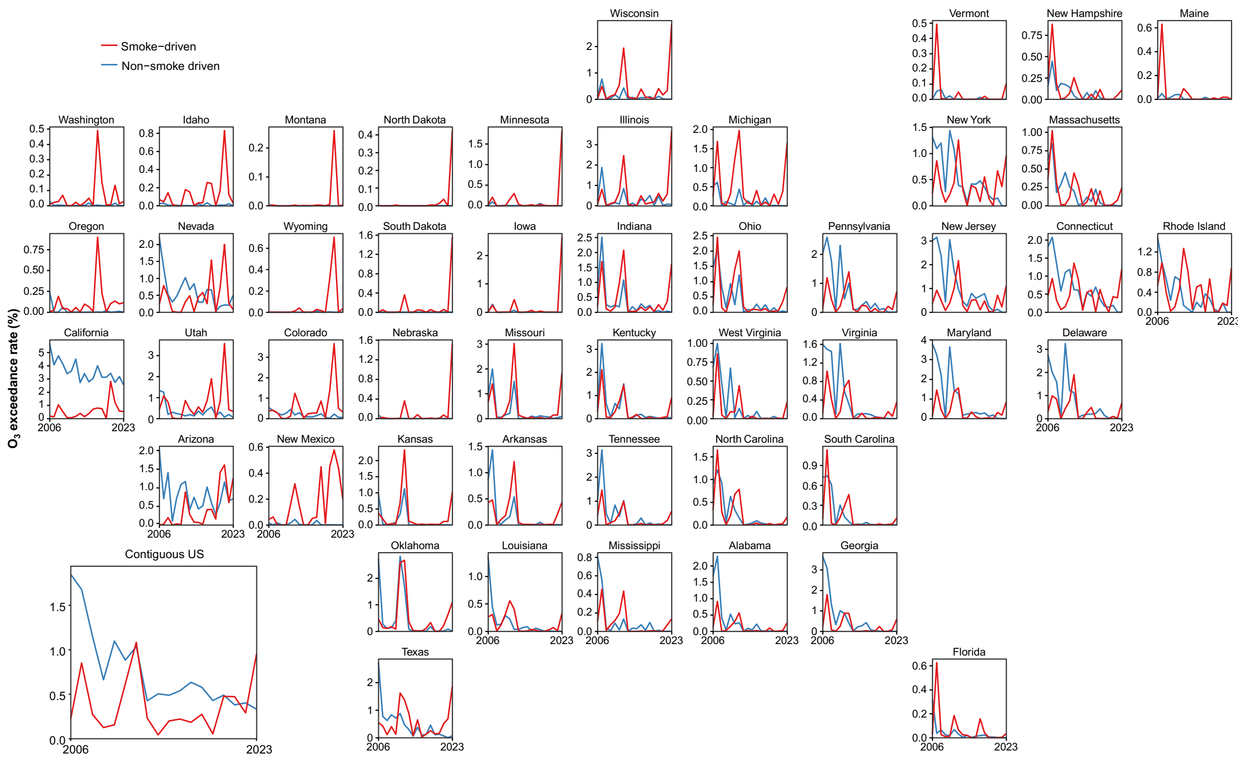

Figure S13: **The influence of wildfire smoke on daily O_3 exceedance.** The plot shows the population-weighted fraction of days with MDA8 $O_3 > 70$ ppb for each state. "Smoke-driven" O_3 exceedance (red) is defined as days when the baseline non-smoke O_3 is below 70 ppb but the total O_3 (smoke O_3 + baseline) exceeds 70 ppb. "Not smoke-driven" O_3 exceedance (blue) is defined as locations and days when the daily non-smoke O_3 already exceeds 70 ppb; thus, the exceedance is not due to fire smoke influences.

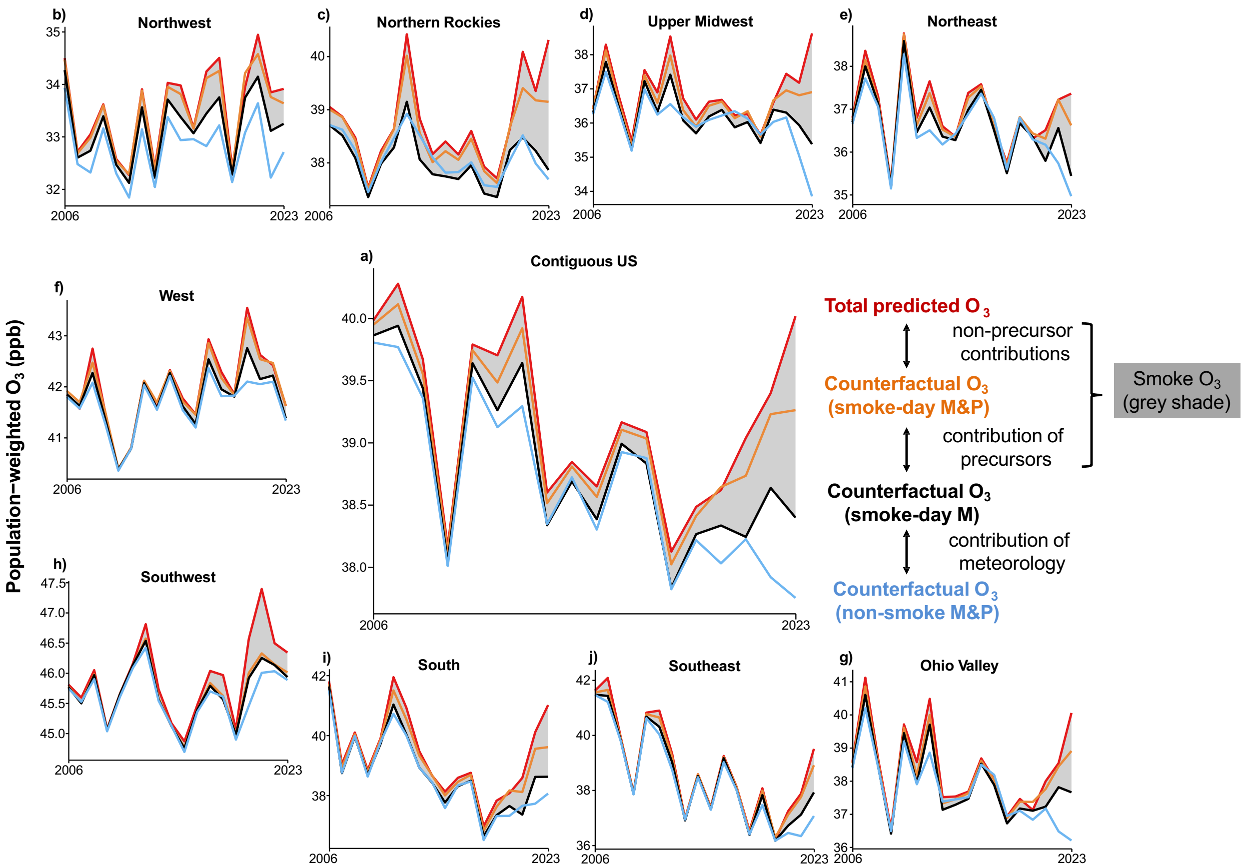

Figure S14: **The influence of fire smoke on population-weighted annual average O_3 across U.S. regions.** Red lines show annual population-weighted averages for predicted total O_3 (both smoke and non-smoke). Orange lines show estimated counterfactual O_3 on smoke days using smoke day meteorology (M) and precursor (P) conditions. Differences between red and orange lines represent the contributions of smoke to O_3 from non-precursor changes. Black lines show estimated counterfactual O_3 on smoke days using smoke day meteorology (M) but average precursor (P) conditions on non-smoke days. Differences between orange and black lines represent the contributions of smoke to O_3 from precursor changes. Blue lines show estimated counterfactual O_3 on smoke days using average meteorology (M) and precursor (P) conditions on non-smoke days. Differences between black and blue lines represent the contributions of meteorological variability to smoke day O_3 concentrations (note this part is not included to quantify smoke O_3 contributions). Gray shading shows the contribution of wildfire smoke to the annual average O_3 calculated by subtracting estimated counterfactual non-smoke O_3 from total O_3 concentrations. The region definition is the same as those in Figure 5.

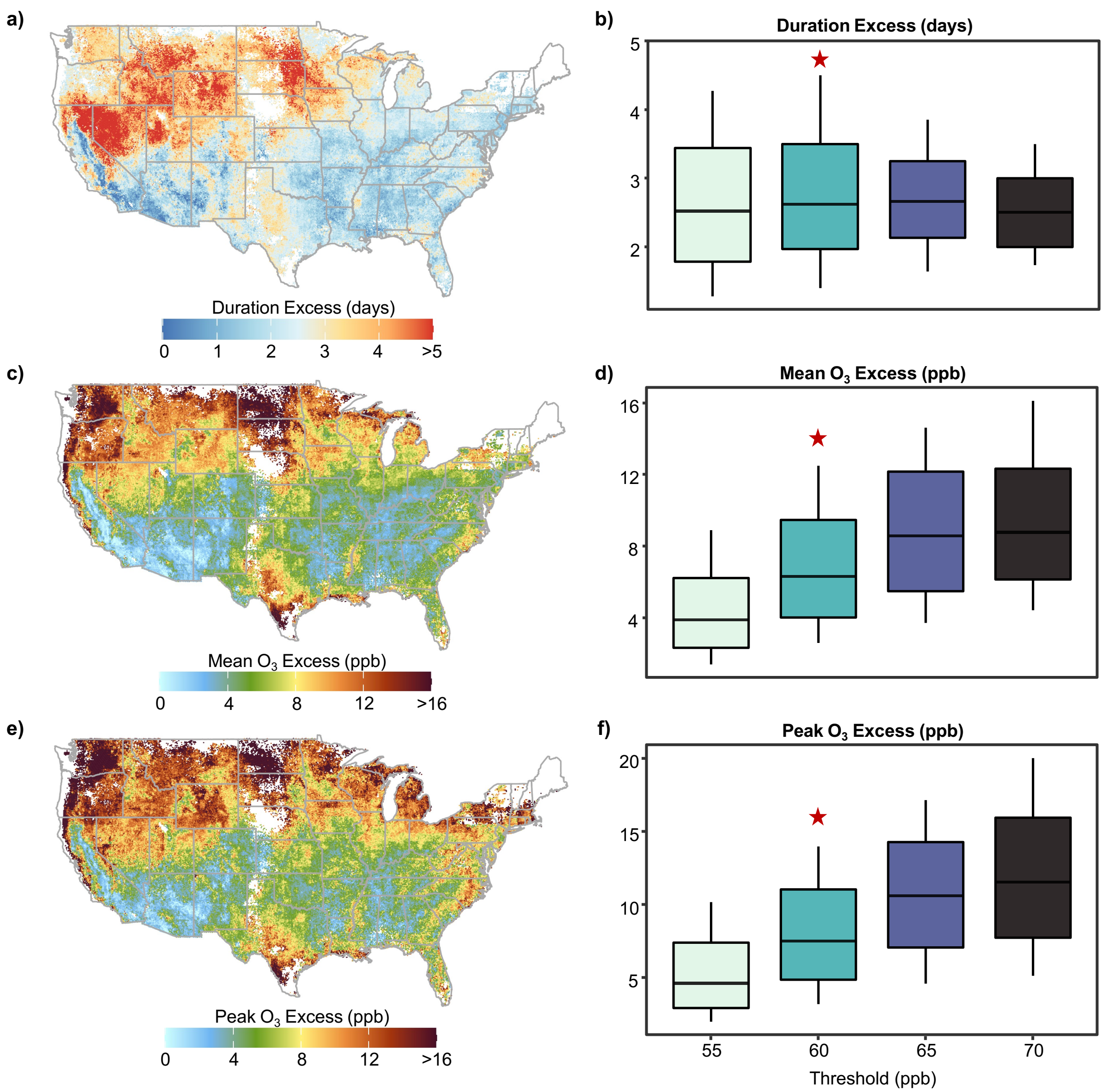

Figure S15: **The influence of wildfire smoke on O_3 extreme episodes.** We define an O_3 extreme episode as at least two consecutive days on which the 3-day mean O_3 concentration exceeds 60 ppb. Throughout, excess refers to the difference between the smoke-influenced value and the non-smoke counterfactual. Panel a: excess duration of O_3 extreme episodes due to wildfire smoke. Panel c: excess mean O_3 concentration during the episode due to wildfire smoke. Panel e: excess peak daily O_3 concentration during the episode due to wildfire smoke. Panels b, d, and f: how the excess duration, excess mean O_3 , and excess peak O_3 change across alternative thresholds for defining an O_3 extreme episode. The main analysis uses a threshold of 60 ppb (denoted by a star).

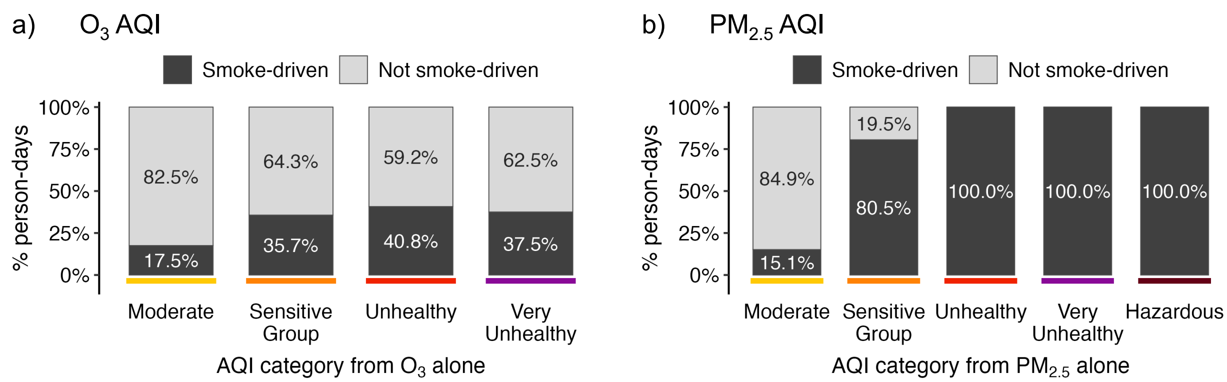

Figure S16: **Contributions of smoke to different sub AQI index of O_3 and $PM_{2.5}$.** The plot shows the percentage of smoke-driven and not smoke-driven person-days in each of five AQI categories (x-axis), 2006–2023, separately for O_3 (panel a) and $PM_{2.5}$ (panel b).

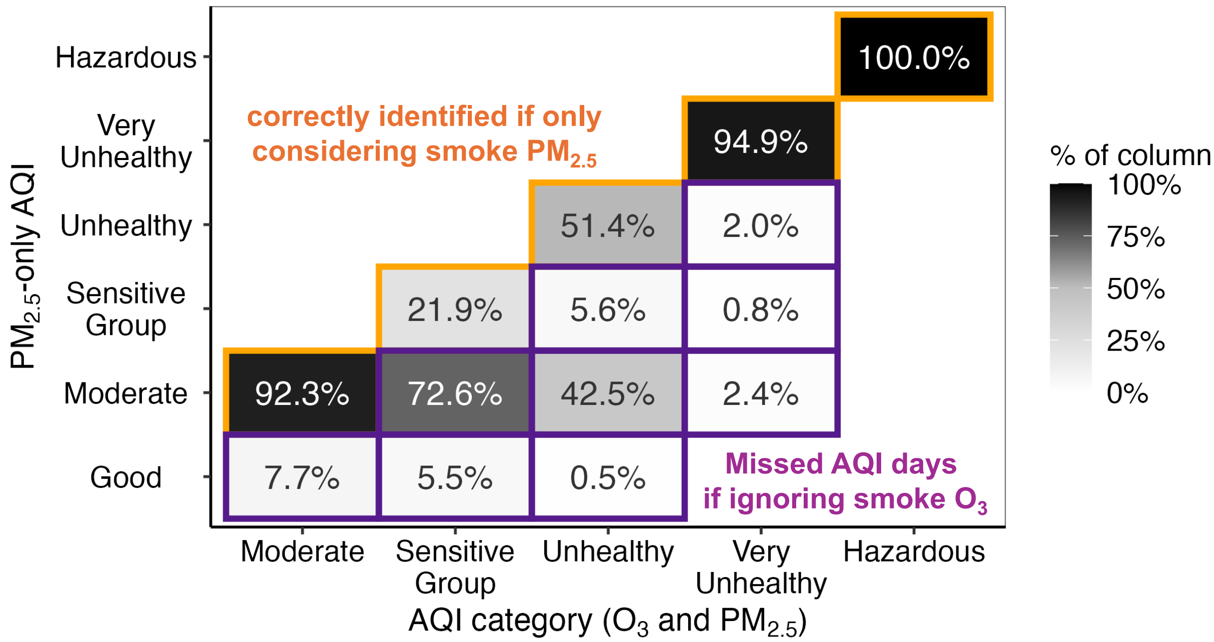

Figure S17: **Misclassification of smoke AQI days if only smoke $PM_{2.5}$ is considered.** The plot shows the distribution of person-days on smoke-driven days across the true AQI category (determined from both $PM_{2.5}$ and O_3, x-axis) and the AQI category that would be reported from $PM_{2.5}$ alone (y-axis). Percentages are calculated within each column, so each true AQI category sums to 100%. Cells on the diagonal (orange) are days for which a $PM_{2.5}$-only AQI reports the correct category. Cells below the diagonal (purple) are the bad AQI days that would be missed if contributions from smoke O_3 were ignored.

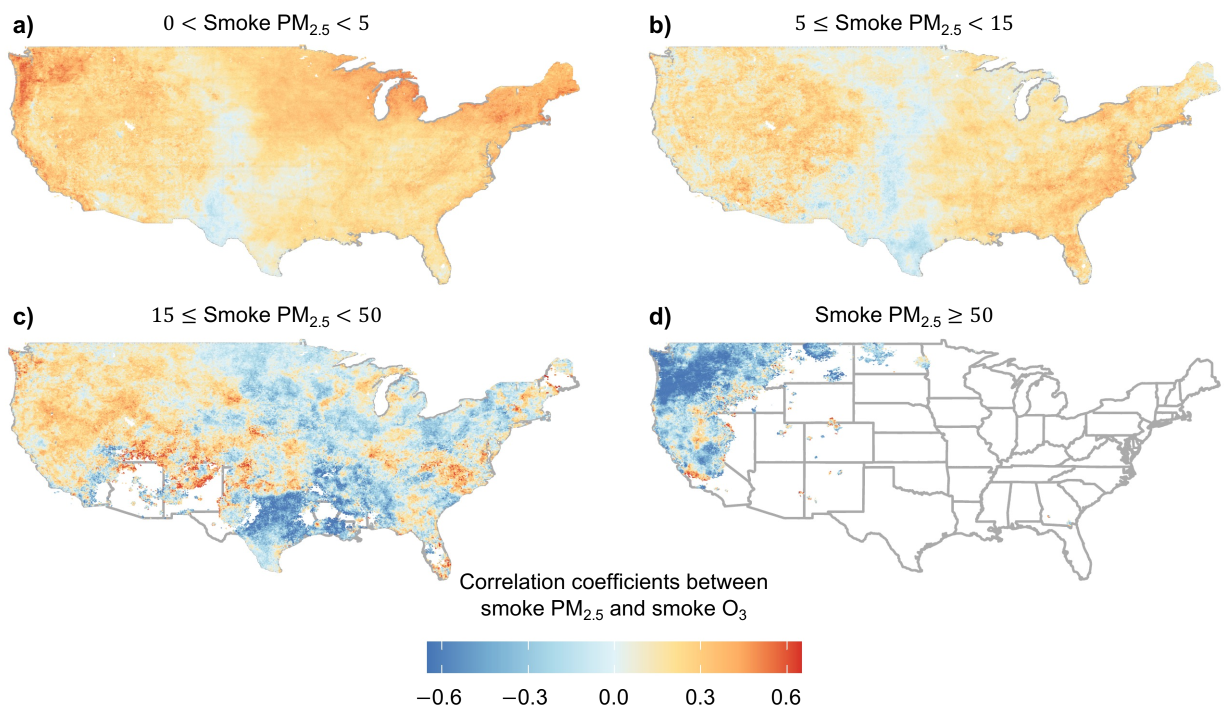

Figure S18: **Varying correlations between daily smoke $PM_{2.5}$ and smoke O_3 across different smoke $PM_{2.5}$ levels.** Panels **a–d** illustrate the Pearson correlation coefficients between daily smoke $PM_{2.5}$ and smoke O_3 within four smoke $PM_{2.5}$ concentration ranges: (**a**) 0–5 $\mu g/m^3$, (**b**) 5–15 $\mu g/m^3$, (**c**) 15–50 $\mu g/m^3$, and (**d**) $\geq$ 50 $\mu g/m^3$.

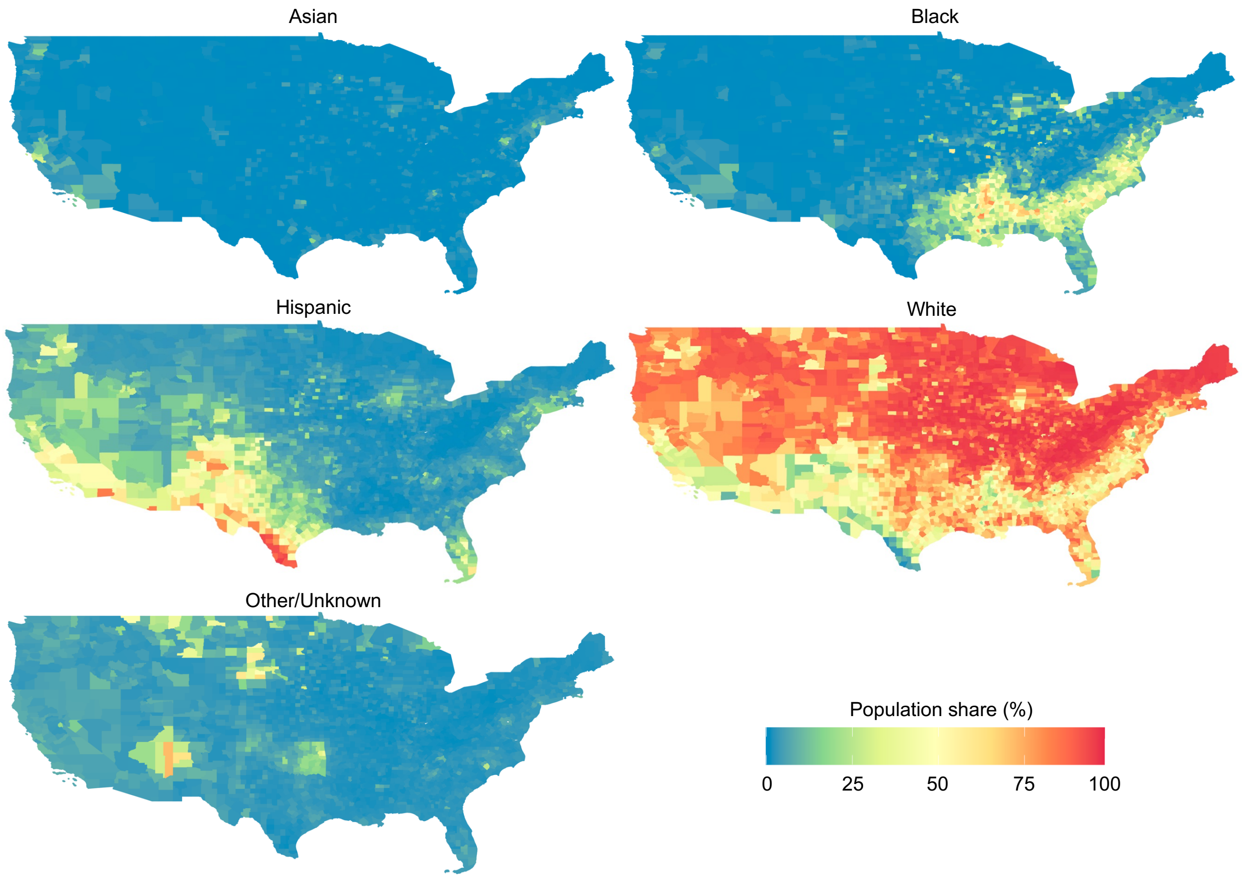

Figure S19: **Geographic distribution of population by race and ethnicity.** The plot illustrates the share of population for the five racial and ethnic groups across the contiguous United States, including Asian, Black, Hispanic, White, and Other/Unknown. The color scale represents the population share (%) within each county belonging to the respective group.

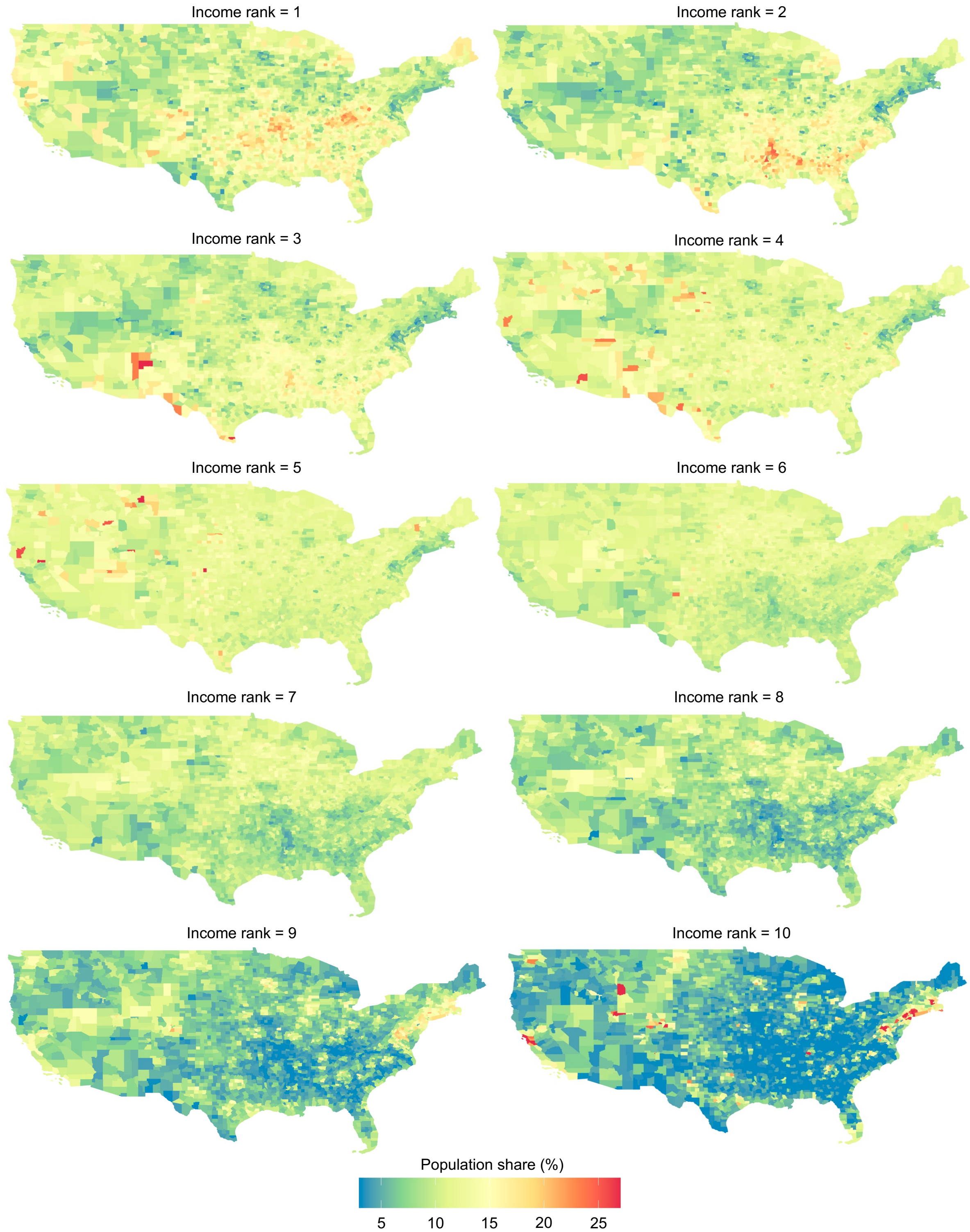

Figure S20: **Geographic distribution of population by income deciles.** Each panel illustrates the share of population for income deciles, ranging from income rank = 1 (lowest income) to income rank = 10 (highest income). The color intensity represents the population share (%) within each county belonging to the respective income decile.

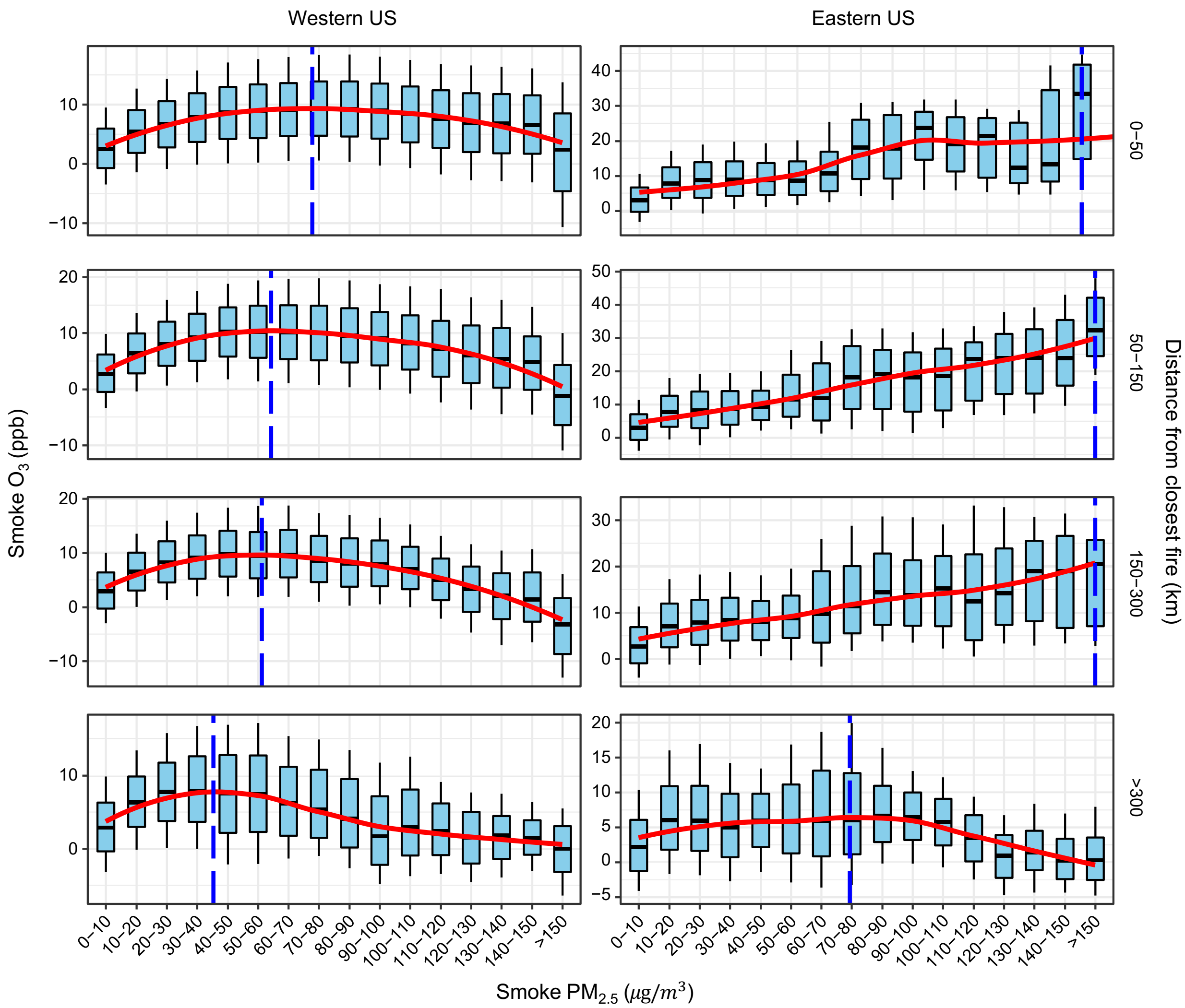

Figure S21: **Non-linear relationship between smoke $PM_{2.5}$ and smoke O_3 across different distances to the closest fire.** The boxplots illustrate the distribution of daily smoke O_3 at different daily smoke $PM_{2.5}$ bins across different distances to the closest fire: thick black lines represent the medians, box edges denote the 25th and 75th percentiles, and whiskers extend to the 10th and 90th percentiles. The solid red lines represent a LOESS regression fitted to the medians of each box. The vertical dashed blue lines indicate the smoke $PM_{2.5}$ threshold at which smoke O_3 concentrations reach their maximum value (i.e. the turning points). Fire distances are calculated as the distance from the grid cell to the closest fire point on the same day.

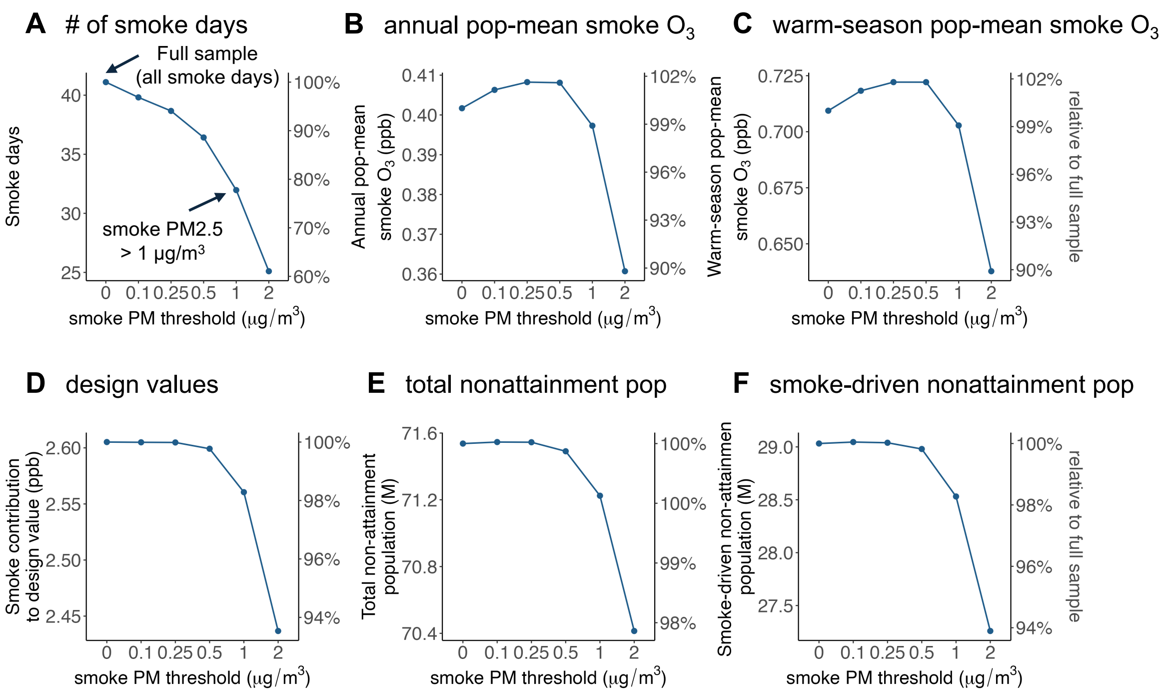

Figure S22: **Results across alternative smoke-day identification thresholds that exclude low smoke $PM_{2.5}$ days from the smoke-day sample**. The plot shows how outcome variables change as the sample is restricted to smoke days with estimated daily smoke $PM_{2.5} > x$ $\mu g/m^3$ (x-axis). Outcomes examined include the number of identified smoke days (panel A), estimated annual and warm-season population-weighted smoke O_3 (B and C), the smoke contribution to annual design values (D), the total population in O_3 nonattainment areas (E), and the additional population in nonattainment areas due to wildfire smoke (F). Smoke $PM_{2.5}$ estimates are derived from Childs et al. 2024 (*56*).